Vascular dysfunction caused by loss of Brn-3b/POU4F2 transcription factor in aortic vascular smooth muscle cells is linked to deregulation of calcium signaling pathways.

Vaishaali Yogendran
Institute of Cardiovascular Science
Laura Mele
Institute of Cardiovascular Science
Oleksandra Prysyazhna
William Harvey Research Institute
Markella Ponticos
UCL Medical School
Vishwanie Budhram-Mahadeo (v.budhram-mahadeo@ucl.ac.uk)
v.budhram-mahadeo@ucl.ac.uk

Article

Keywords: Brn-3b TF, knockout mice, VSMC, calcium channels, sarco-endoplasmic reticulum, vascular contractility, SERCA, RyR, vascular dysfunction, immune responses

Posted Date: January 16th, 2023

DOI: https://doi.org/10.21203/rs.3.rs-2402366/v1

Additional Declarations:
Table 1 and 2 are available in the Supplementary Files section.

Vascular dysfunction caused by loss of Brn-3b/POU4F2 transcription factor in aortic vascular smooth muscle cells is linked to deregulation of calcium signaling pathways

Vaishaali Yogendran[1*], Laura Mele[1*], Oleksandra Prysyazhna[2], Markella Ponticos[3] and Vishwanie S. Budhram-Mahadeo[1*¶]

[1]Molecular Biology Development and Disease, UCL Institute of Cardiovascular Science, London, UK

[2]Clinical Pharmacology Centre, William Harvey Research Institute, Queen Mary University of London, UK

[3] UCL Medical School, Royal Free Campus, Rowland Hill Street, Hampstead, London, UK

Running title: Loss of Brn-3b affects VSMC fate and function

Corresponding author:
Prof Vishwanie Shanie Budhram-Mahadeo

Molecular Biology Development and Disease Laboratory,

Department of Preclinical and Fundamental Sciences

UCL Rayne Building; 5 University Street; London WC1E 6JF

Keywords: Brn-3b TF, knockout mice, VSMC, calcium channels, sarco-endoplasmic reticulum, vascular contractility, SERCA, RyR, vascular dysfunction, immune responses

Abstract:

Phenotypic and functional changes in vascular smooth muscle cells (VSMCs) contribute significantly to cardiovascular diseases (CVD) but factors driving early adverse vascular changes are poorly understood. We report on novel and important roles for the Brn-3b/POU4F2 (Brn-3b) transcription factor (TF) in controlling VSMC integrity and function. Brn-3b protein is expressed in mouse aorta with localisation to VSMCs. Male Brn-3b KO aortas displayed extensive remodelling with increased extracellular matrix (ECM) deposition, elastin fiber disruption and aortic coarctation. RNA sequencing analysis showed that these effects were linked to deregulation of genes required for calcium (Ca^{2+}) signaling, vascular contractility, sarco-endoplasmic reticulum (S/ER) stress responses and immune function in Brn-3b KO aortas and validation studies confirmed changes in Ca^{2+} signalling genes linked to increased intracellular Ca^{2+} and S/ER Ca^{2+} depletion [e.g. increased, Cacna1d Ca^{2+} channels; ryanodine receptor 2, (RyR2) and phospholamban (PLN) but reduced ATP2a1, encoding SERCA1 pump and chaperone proteins, Hspb1, HspA8, DnaJa1 linked to increased S/ER stress, which also contributes to contractile dysfunction. Accordingly, vascular rings from Brn-3b KO aortas displayed attenuated contractility in response to KCl or phenylephrine (PE) while Brn-3b KO-derived VSMC displayed abnormal Ca^{2+} signalling following ATP stimulation. This data suggests that Brn-3b target genes are necessary to maintain vascular integrity and contractile function and deregulation upon loss of Brn-3b will contribute to contractile dysfunction and CVD.

Introduction:

Adverse vascular changes that reduce arterial compliance and contractility are major contributors to cardiovascular diseases (CVD), a leading cause of morbidity and mortality, globally[1-3]. In fact, increased arterial stiffness and reduced contractility are recognised as independent predictors of CVD mortality, particularly in patients with essential hypertension[4-6]. However, chronic CVD are associated with vascular changes that occur gradually over time but often remain asymptomatic until later stages, when irreversible vascular damage and arterial stiffening has already occurred[2, 7]. Consequently, the factors that drive early vascular changes are not well understood. Therefore, elucidating the mechanisms controlling vascular integrity and function in healthy blood vessels (BV) can help to provide insight into pathophysiological processes that cause vascular dysfunction and disease.

Large BVs, such as the aorta, are uniquely adapted for sensing and responding rapidly to pulsatile blood flow and large changes in cardiac output and blood pressure, under different conditions[8]. Vascular smooth muscle cells (VSMCs), which are located in the tunica media (TM) of BV are essential for maintaining vascular tone and BV diameter and thereby affect blood flow and pressure[9, 10]. In normal BV, differentiated VSMCs express contractile proteins such as smooth muscle protein 22-alpha (SM22α), alpha smooth muscle actin (α-SMA) and calponin that control vascular tone[11] but also produce elastin (Eln), which confers elastance and recoil and for adaptation to large changes in blood flow[8, 12]. Contraction of differentiated VSMCs is controlled by changes in intracellular calcium (Ca^{2+}) levels, which is actively regulated through Ca^{2+} channels, pumps or other regulatory proteins found in the plasma membrane or on the sarco-endoplasmic reticulin (S/ER)[13-15]. Under normal conditions, membrane depolarisation increases Ca^{2+} influx via the plasma membrane by activating L-type voltage-gated Ca^{2+} (CaV) channels, thereby raising intracellular calcium levels. This can also

be increased by Ca^{2+} release from S/ER intracellular store either via inositol triphosphate (IP_3) receptors or via ryanodine receptors (RyR), which contributes to localised Ca^{2+}increases (Ca^{2+} transient or sparks)[16, 17]. Raised intracellular Ca^{2+} drives VSMC contraction by driving calmodulin mediated activation of myosin light chain kinase (MLCK) and phosphorylation of myosin light chain (MLC), resulting in actin-myosin interaction[11, 18]. Conversely, membrane re-polarisation and VSMC relaxation depends on reduction of intracellular Ca^{2+} levels by its re-uptake into intracellular stores by S/ER Ca^{2+}ATPase (SERCA) pumps (encoded by ATP2a genes)[19], or by efflux via plasma membrane Ca^{2+} (PMCA) pumps, encoded by ATP2b genes[13, 15, 20]. Ca^{2+} reuptake into the S/ER can also be highly regulated by phospholamban (PLN) which inhibits SERCA pump activity. Therefore, changes in genes regulating intracellular Ca^{2+} levels can cause contractile dysfunction in VSMCs[13, 15, 20].

In VSMCs, contractile function and responses are highly dependent upon the cell phenotype. This is because the inherent plasticity of VSMC means that vascular damage caused by chronic stress [e.g. raised intracellular Ca^{2+} or S/ER Ca^{2+}depletion and stress; increased reactive oxygen species (ROS), inflammation[21-25]] can trigger phenotypic switching whereby cells undergo de-differentiation and switch from contractile cells into mesenchymal phenotypes that acquire migratory, proliferative and secretory properties[12, 14]. Such effects are driven by changes in the expression of genes that encode important cellular proteins e.g. reduced contractile proteins and increased extracellular matrix (ECM) proteins e.g. collagen which affects VSMC contractility and contributes to vascular dysfunction such as arterial stiffening and hypertension[10, 14]. Gene expression itself is highly regulated, especially at the level of transcription where tissue-specific TFs that activate or repress the expression of multiple target genes can control cell fate[26]. Therefore, identifying TFs which regulate genes

that control normal vascular integrity and function can provide insight into the mechanisms underlying adverse vascular changes and progression to CVD[27].

The Brn-3b/POUF2 protein (Brn-3b) is POU domain homeodomain TF, characterised by a highly conserved DNA binding POU (pit-oct-unc) domain that binds to unique BRNF binding in the promoter/enhancer of target genes. Brn-3b was originally isolated from neuronal cells and therefore widely studied in the central and peripheral nervous system including retinal ganglion cells (RGC). However, it was also subsequently detected in many other tissues including cardiovascular system (cardiomyocytes/heart), metabolic tissue (skeletal muscle and adipose tissue) and immune cells [peripheral blood mononuclear cells (PBMC), T-cells and monocytes)] [28]. Importantly, Brn-3b can mediate complex tissue-specific effects by regulating the expression of diverse subsets of genes that control many cellular processes including proliferation, metabolism, differentiation and apoptosis and these effects can be mediated directly or indirectly, depending on the cell type and growth conditions[28-31]. Direct effects of Brn-3b can arise when this TF binds to unique BRNF DNA sites in the gene promoters and then either activate or repress gene transcription by RNA polymerase II (RNAPII), depending on cell/tissue type[32-34]. For instance, Brn-3b controls RGC survival and differentiation by regulating sonic hedgehog (Shh), myostatin (Gdf8) and Pax4[35, 36]. However, in epithelial-derived tumour cells, Brn-3b promotes cell proliferation by activating cell cycle proteins, cyclinD1 and CDK4 while repressing the Brca1 tumour suppressor gene[37, 38]. Yet in metabolic tissues including skeletal muscle and adipose tissues, Brn-3b is implicated in regulation of glucose homeostasis by controlling expression of Glut4 and GSK3β since reduction or loss of Brn-3b is linked to hyperglycaemia and insulin resistance[30].

However, Brn-3b can also regulate gene transcription indirectly by binding to and modulating the effects of other TF including by interacting and modulating the transcriptional effects of other regulators including p53 tumour suppressor protein and estrogen receptor (ER) on their target genes [28, 31, 33, 39]. For instance, if co-expressed with p53, Brn-3b interacts and cooperates with p53 to enhance transcription of pro-apoptotic genes such as Bax, Noxa and Puma, thereby increasing apoptosis[26, 27]. In contrast, Brn-3b interacts and cooperates with ER to increase Hsp27 (HspB1), thereby enhancing cell survival, differentiation or motility[28, 34]. Thus, Brn-3b can drive complex effects on gene expression and cell fate depending on growth conditions, interaction and co-expression with other regulators.

More recent studies have identified key roles for Brn-3b in controlling responses in cardiomyocytes of the heart. Brn-3b is highly expressed in foetal hearts, with lower levels found in normal adult hearts. However, studies in hearts from male Brn-3b KO have identified subtle differences in contractility and cardiovascular function at baseline e.g. reduced arterial elastance and end systolic pressure volume relationship (ESPVR)[29]. Moreover, Brn-3b is highly re-expressed in cardiomyocytes following acute injury (e.g. coronary artery ligation)[31] or in response to chronic stress (e.g. AngII treatment), which induces ventricular hypertrophy[29]. In the latter model, Brn-3b is necessary for normal adaptive responses in male hearts because AngII treatment induced adverse functional responses in Brn-3bKO mutants which was associated with reduced cardiac output and ejection fraction linked to extensive fibrosis in the ventricular wall and remodelling around the coronary vasculature[29].

Extensive remodelling in coronary arteries of Brn-3b KO mice suggested that loss of Brn-3b may also affect vascular integrity and function[35]. This is particularly interesting in light of published genome wide association studies (GWAS) data identifying SNPs associated with

coronary heart disease (CHD), coronary artery diseases (CAD) and cerebrovascular accident (CVA) within the genomic region chromosome 4q (31.2), containing the Brn-3b genomic locus[40-45]. However, to our knowledge, the expression and effects of Brn-3b in the vasculature are still unknown.

In this study, we provide evidence to show localisation of Brn-3b expression in aortic VSMCs and studies using male Brn-3b KO mice showed that its loss is linked to significant histological and structural changes in the aorta, including coarctation, thickening of the tunica adventitia (TA) and disrupted Eln fibres. Such effects were associated with decreased lumen diameter and increased wall stiffness and attenuated contractile responses to KCl, PE and U46619 treatment in Brn-3b KO aortas. RNA sequencing analysis of aortas from Brn-3b KO and WT mice showed that genes regulating Ca^{2+} signalling pathways were most significantly affected by loss of Brn-3b followed by VSMC contractility, S/ER stress and immune responses. qRT-PCR validation studies were focused on confirming changes in genes involved in Ca^{2+} signalling and stress responses because of abnormal contractility observed in mutant aortas. Results showed that loss of Brn-3b caused increased mRNA encoding voltage-gated Ca^{2+} channels, Cacna1d; S/ER Ca^{2+} channel, rayanodine receptor RyR2 which controls Ca^{2+} release from S/ER while increased regulatory Pln and reduced Atp2a1 are likely to contribute to S/ER Ca^{2+} depletion and raised intracellular Ca^{2+}. Such changes combined with reduced chaperone genes e.g. Hsph1, Hspb1, DnajA1 will increase ER stress[25, 46], which can trigger phenotypic switching and abnormal contractility. Taken together, these results suggest that Brn-3b TF controls genes that are required for maintaining calcium homeostasis, contractility and stress responses in VSMCs and loss of Brn-3b will lead to vascular dysfunction.

Materials and Methods:

Materials: General laboratory reagents: Merck (Nottingham, UK) and Sigma (Dorset, UK), unless otherwise stated. Primary antibodies: Brn3b-rabbit pAb (Abcam-Cambridge, UK); GAPDH and β-tubulin (Cell Signalling Technology, USA) α-SMA (Abcam-Cambridge, UK) Col1a1 (Abcam, Cambridge, UK). HRP-conjugated secondary Ab, Dako (Cambridgeshire, UK).

qRT-PCR Primer Sequences:

Brn-3b F - 5' GAGAGAGCGCTCACAATTCC 3';
Brn3b R- 5' ATGGTGGTGGTGGCTCTTAC 3'

36b4 F- 5' AGATGCAGCAGATCCGCAT 3';
36b4 R- 5' GTTCTTGCCCATCAGCACC 3'

GapdhF- 5' CTTCATTGACCTCAACTAC 3';
Gapdh R 5' AGTGATGGCATGGACTGTG 3'

Ryr1 F- 5' GCAGGAGACGTACAGTCAGG 3';
Ryr1 R – 5' CAAGGATGTCTGCACGGAGT 3'

Ryr2F-5'CCTACAGTGGTATGTATCTTTGCTGTCT3';
Ryr2R- 5'CTCTTGAAGGCCAACATC GAA 3'

Cacna1dF-5'CGTGCCTTCCGAGTGTTAAG3';
Cacna1dR-5'GGACCATGGCTTTTATAATGGA 3'

Cacnb2F- 5'TGGAGTCGACTTTTTGCCGA 3'
Cacnb2 R- 5' TCCATAGGACTGTGCTCCGA 3'

Pln F- 5' ACCGAAGCCAAGGTCTCCTA 3';
Pln R- 5' TAGCCGAGCGAGTGAGGTAT 3'

DnaJa1 F- 5' CCGCTCACCGGCTGTAAA 3';
DnaJa1 R- 5' GGGTGGTACTTCAAGGCCAA 3'

Hspa8 F- 5' CTGCTGCTATTGCTTACGGC 3';
Hspa8 R- 5' TCAAAAGTGCCACCTCCCAA 3'

Hsph1 F- 5'AACCCCAGATGCTGACAAAG 3';
Hsph1 R- 5'GCAGCTCAACATTTACCACCT 3'

Atp2A1 F- 5'AAGGCTCGGGACATCGTT 3';
Atp2A1 R- 5'GGATGTCTGCAGGGACTTTG 3'

Methods:

Experimental models: All animal experiments were carried out in compliance with UK Home Office regulations (Animals Scientific Procedures Act 1986) and approved by local UCL Ethics Review Board. Early studies used Wistar rats or wild-type (WT) C57Bl/6 mouse models purchased from commercial companies (Harlan UK). Later studies with knockout (KO) mice and WT littermate controls were obtained by crossing Brn-3b heterozygotes C57Bl/6 strains.

Histological staining: To analyse for morphological and structural changes in the aortic sections, histological staining was undertaken using Haematoxylin and Eosin (H & E) staining; Masson's trichrome staining (Abcam-Cambridge, UK) or oil red O staining (Sigma, UK). For these studies, formalin-fixed, paraffin-embedded aortic sections from age matched Brn-3b KO and WT mice, were dewaxed, rehydrated and stained according to the manufacturer's protocol. To quantify TA thickness matched aortic sections were analysed using NDPview-2 software (Hamamatsu, Japan), by undertaking ~50 equidistant measurements of the aortic wall. Data represents mean $\pm$ SD from $\geq$6 matched, independent WT or Brn-3b KO aortic sections

Protein preparation and quantification:

Total cellular protein extracts from mouse or rat aortas or cultured VSMC were prepared in RIPA buffer using standard protocols[29] and quantified using BCA (bicinchoninic acid) kit (Merck, UK). ~30μg/well protein extracts were resolved on SDS-PAGE gels and transferred onto PVDF membranes overnight[31]. Following incubation (1 hour at RT) with block buffer [4%milk + phosphate buffered saline + 0.1% Tween-20 (PBST)], and primary antibody for 2 hours at RT or overnight at 4^{o}C; membranes were washed (X5) then incubated with HRP-conjugated 2nd antibody (1hour; RT). Signals were developed using enhanced chemiluminescence (ECL) (BioRad, UK) on Syngene G:BOX imager and protein quantification

done out using Fiji (ImageJ) software. Variation in protein loading was adjusted with β-tubulin (housekeeping protein).

Co-immunostaining using colorimetric or fluorescent detection

Immunostaining for protein localisation was done using paraffin-embedded tissue sections or cultured cells. Tissue sections were dewaxed and rehydrated prior to antigen retrieval (0.01M sodium citrate pH6.0, 10 minutes), and single or double immunostaining protocols undertaken using Vectastain Elite ABC Kit (Vectorlabs) or ImmPRESS® Duet Double-Staining Kit, (according to the manufacturer's protocol[29, 39]). Primary antibodies were incubated in a humidified chamber, either 2 hours (RT) or overnight (4°C) and control samples were incubated with second antibody only. The manufacturers protocol was modified to include additional washes (5 PBST; 5minutes) after which detection was undertaken using Vectastain Elite ABC Kit (Vectorlabs) or ImmPACT® DAB EqV Substrate (HRP, brown); ImmPACT Vector® Red Substrate (AP, magenta). Following graded ethanol dehydration, cover-slipped slides were imaged using the Hamamatsu Nanozoomer (Hamamatsu, Japan) then analysed using NDP view 2 software.

Fluorescent immunostaining of cultured cells was undertaken as previously described[31]. Briefly cells were fixed in 4% PFA and permeable if necessary. Following incubation with block solution (20% goat serum in PBST) antibodies were incubated either overnight at 4° C or 2 hours at room temperature. Following 5X washes in PBST and incubation with appropriate fluorescent tagged, secondary Ab, cells were imaged using fluorescent microscopy and Leica software for analysis (Leica DMi8, LAS X).

Transmission Electron Microscopy

Transmission electron microscopy (TEM) were undertaken using resin embedded sections prepared from Brn-3b KO mutant aortas and wild-type controls using well established methods.

Briefly, aortas were perfused and fixed in100 mM cacodylate buffer containing 2.5% glutaraldehyde overnight at 4ºC. Samples were transferred to 1% osmium tetroxide, dehydrated in an ethanol series, and then embedded in araldite resin (Electron Microscopy Sciences, Hatsfield, PA). 0.5 µm sections were stained with toluidine-blue and analyses using light microscopy. For electron microscopy, ultra-thin sections (70-80 nm) were cut and set on 200-mesh copper. The grids were counterstained with lead citrate for 3 mins and imaged on a Jeol 1400 electron microscope with a Rio Gatan camera.

RNA sequencing and data analysis:

For RNA sequencing, total RNA was prepared from aortas taken from Brn-3b KO male mutants and age-matched wild-type controls (>3/set). Quality controls (QC) was done using NanoDrop and Agilent Bioanalyser 2100 before library preparation was carried out using KAPA mRNA HyperPrep Kit (p/n KK8580) according to manufacturer's instructions. During this process, highly purified mRNA, fragmented by chemical hydrolysis and primed with random hexamers, was used for RNA-dependent cDNA synthesis with "A-tailed" at 3' end, to prevent self-ligation and adapter dimerisation. Amplification and first strand library preparation was undertaken using adapters for PCR with high fidelity polymerase and libraries were sequenced on the NextSeq 500 instrument (Illumina, San Diego, US) using either a 43bp or 81bp paired end run with general yield of ~15 million reads per sample. De-multiplexed data converted to Fastq files (Illumina's bcl2fastq Conversion Software v2.19) were used for alignment with the reference genome using STAR (v2.5b) and aligned data were deduplicated (Picard Tools v2.7.1) and reads per transcript counted by FeatureCounts (v1.4.6p5). Ensembl ID for each gene was determined using g:Profiler and this data was then used for normalisation, modelling and differential expression analysis using the iDEP.93 software platform, which connects

multiple R/Bioconductor packages with annotation and pathway databases to provide comprehensive analysis of RNA sequencing data

Data analysis using iDEP.93 platform

Preprocessing was done to filter genes with ≥0.5 counts per million in at least one sample inclusion in the analysis using EdgeR (default settings CPM-0.5, pseudo-count c-4) and principal component analysis was undertaken using PC1 and PC 3 to visualise the relationship between sample groups based on sample variance. For K-means clustering analysis, read counts were transformed to $\log_2$ and the 2500 most variable genes (based on standard deviation ranking) were separated into one of 4 clusters, based on functionality, molecular and biological processes with students t-test used to calculate the values for enriched pathways within each cluster. KEGG (Kyoto Encyclopedia of Genes and Genomes) pathway analysis provided a systematic analysis of pathways associated with genes in each cluster (adjusted p-value). Similarly, Gene Ontology (GO) database platforms provided information on the association of genes within each cluster with specific biological processes, molecular function and cellular components. The Disease.Jensen.DISEASES database also linked to this platform, was used to identify diseases associated with specific subsets of genes, depending on adjusted p values. Gene Set Enrichment Analysis (GSEA) was undertaken to identify genes that were either up- or down-regulated in Brn-3b KO vs WT, using the DESeq2 method, which calculated the p-values using the Wald test and used the read count data (unlike K-Means Clustering which uses transformed data). Analyses were undertaken using absolute values of fold changes in the pre-ranked mode (preranked fgsea) and were based on comparison between genotypes i.e. KO vs WT, with 15 – 2000 gene set (min; max), pathway significance cut-off of 0.1 FDR and minimum fold change of 1.5, with top 30 pathways selected. Normalised enrichment score (NES) accounted for gene set sizes and correlations between gene set and

expression data, with positive and negative enrichment scores (ES) indicating correlation with Brn-3b KO and WT phenotypes respectively. KEGG and GO pathway analyses were used to determine functional changes associated with up- or down-regulated gene sets.

Differential Expression of Genes (DEG) was also carried out using DESeq2 method to identify genes with significant and concordant differences in a-priori gene sets in the different variables (Brn-3b KO vs WT). The minimum fold change was set at 1.5 and false discovery rate (FDR) cut off was 0.10. WT was used as the control baseline for the analyses. Functionality of up and/or downregulated was determined using g:Profiler.

Primary VSMC cultures:

Primary VSMC cultures were prepared from freshly dissected Brn-3b KO and WT aortas as described[47]. Briefly, excess perivascular tissue and tunica adventitia were carefully removed from isolated aortas (to prevent contamination with fibroblast of PVAT) and ~2mm of cleaned aortic rings were carefully placed into a T25 flask, in large drops of growth medium (DMEM-F12+1% Penicillin-Streptomycin +15%fetal calf serum) and left to attach to the flask. After 5-10 min, culture medium was gently added to cover flask, which was then placed in a humidified incubator (37° C and 5% $CO_{2)}$. Media were changed every 2-3 days until cells were confluent and ready for experiments (up to 10 -14 days).

Gene validation: RNA extraction, cDNA synthesis and quantitative polymerase chain reaction (qRT PCR): RNA was extracted from snap-frozen aortas taken from Brn-3b KO and WT aortas. Tissues were crushed in liquid nitrogen and homogenised in RLT buffer then RNA was extracted using Qiagen RNeasy mini kit (Qiagen, Manchester, UK) or TRIZOL® Reagent (Invitrogen). Since Brn-3b(s) is only encoded by exon 2, it was not possible to use primers spanning the intron. As such, it was necessary to remove all contaminating genomic DNA prior

to cDNA synthesis, which was achieved using RNAse-free DNAse1 (Promega, Southampton, UK). 1μg of total RNA from each sample was used for cDNA synthesis, using Superscript™ II Reverse Transcriptase (Invitrogen, UK), according to the manufacturer's protocol.

Validation studies to confirm changes in RNA sequencing data for selected genes was undertaken using q-RT-PCR with Eppendorf Mastercycler using SYBR Green chemistry. Primers designed for each target gene were used to amplify cDNA for specify genes using independent WT or KO aortic RNA. Housekeeping genes e.g. GAPDH and 36B4 were used correct for RNA variability between samples and a reference sample was included to facilitate use of ΔΔCT method to calculate fold changes in relation to controls samples. Statistical analysis was undertaken using results from multiple experiments using independent aortas with student's t-test used to show significance, *$p \leq 0.05$.

Wire Myography for contractility studies in Brn-3b KO & WT aortic vascular rings:

Thoracic aorta from Brn-3b KO and WT mice were prepared by removing perivascular vascular tissue. The cleaned aortae were used to generate vascular rings for wire myography during which tissues were bathed in Krebs solution at 37°C with a 95% O_2 and 5% CO_2 environment. Vascular rings were mounted on the myograph (Danish Myo Technology, Hinnerup, Denmark) and DMT normalization module used for isometric tension recordings. At baseline, the optimal pre-tension condition established by stretching to 95% internal circumference with resting transmural pressure of 100mmHg (IC100). Following equilibration and normalisation of vascular reactivity, constricting cumulative dose-responses were measured following treatment with potassium chloride (KCl, 7.50 mM/L to 90 mM/L), phenylephrine (PE, 100 nM/L to 100 μM/L) (Sigma-Aldrich, Missouri, USA) and U-46619 (0.1 nM/L-25 nM/L) (Cambridge Biosciences, Cambridge, UK). Results shown at raw force (mN)[48, 49].

Results:

Brn-3b expression and localisation in the aorta and primary VSMC cultures:

Mouse aortas were used to analyse for Brn-3b expression in the vasculature using either blot (WB) analysis or immunostaining. Fig1a shows that Brn-3b(s) protein isoform was readily detectable in aortic protein extracts from WT mice but not in Brn-3b KO aortic extracts (full blot in Supplementary Fig 1). Similarly, immunostaining showed Brn-3b protein expression in the medial layer of aortic sections (brown), where it was co-localised with the VSMC marker, α-SMA (magenta) (Fig 1b), when compared with the control (2^{nd} Abs). In addition, co-immunofluorescent of isolated primary mouse aortic VSMC cultures showed Brn-3b antibody staining (green) co-localised in α-SMA-expressing (red) VSMC derived from WT aortas (top panel) where DAPI staining (blue) of cell nuclei, showed Brn-3b expression in the nuclear and perinuclear regions in aortic VSMCs. However, as expected, Brn-3b was undetectable in VSMC from Brn-3b KO mutant aortas (bottom panel).

Abnormal structural and histological changes in Brn-3b KO aorta:

Since loss of Brn-3b was linked to extensive remodelling around the coronary arteries in male Brn-3b KO hearts[29], we next analysed for changes in aortas from male Brn-3b KO mice compared with WT controls. Fig 2a shows that aortas from Brn-3b KO mice displayed small but consistent narrowing/coarctation in the descending aortas, when compared with age and gender-matched WT controls. H&E staining of aortic sections also showed marked histological changes in Brn-3b KO aortas (Fig 2b), which included thickening of the adventitial (TA) layer and increased white adipose tissue (WAT) deposits in the perivascular adipose tissues (PVAT), when compared with WT aortas. In addition, Masson's trichrome staining showed that TA thickening in Brn-3b KO aortas was linked to the increased deposition of ECM proteins (blue)

(fig 2c-d) and this was confirmed by immunostaining for collagen 1A1 (Col1a1) protein (fig 2d). Disruption of elastin fibres in the mutant aortas can be observed in trichrome staining (fig 2f) and this was confirmed using van Gieson staining (fig 2g).

Fig 2g(i) shows that quantification of aortic cross-sections from independent age-and gender matched WT or Brn-3b KO aortas (n>6) identified significant increases in TA thickness in Brn-3b KO aortas. In addition, measurement of lumen diameter in transverse aortic sections showed reduction in Brn-3b KO when compared with WT aortas (ii). Immunostaining of aortic sections also confirmed increased col1a1 protein expression in Brn-3b KO aortas, when compared with WT controls (Fig 2f). Such structural and histological changes in mutant aortas strongly suggest that loss of Brn-3b can profoundly alter aortic structure and morphology.

Representative images obtained using transmission electron microscopy confirmed the abnormal changes in mutant aortas with fig 3a showing that increased thickness in the adventitial layer of Brn-3b KO aortas was linked to increased collagen deposition when compared with WT aortas. Similarly, disruption in the elastin lamina in mutant aorta can be clearly seen in fig 3b while fig 3c shows differences in fat cells but also highlights infiltration of immune cells (arrows) in aortic PVAT from Brn-3b KO that was not evident in PVAT from WT aortas. These results identified the ultrastructural changes associated with morphological abnormalities seen in Brn-3b KO aortas.

Contractile changes in Brn-3b KO aorta:

To determine if structural changes in Brn-3b KO aortas affected aortic blood flow, echocardiography was undertaken using Visualsonics Vivo 2100. Figure 4a shows that male Brn-3b KO mice displayed increased ascending aortic velocity when compared with age-matched WT controls, despite no significant differences in aortic root diameter (figure 4b), suggesting potential changes on aortic contractility. Therefore, wire myography was used to

assess for differences in elastic properties of vascular rings taken from WT and Brn-3b KO aortas. Baseline wall stiffness in aortic rings was established using the normalisation method whereby vascular rings were pre-stretched to 95% of internal circumference with resting transmural pressure of 100 mmHg (IC 100). Interestingly, IC100 values were significantly lower in Brn-3b KO vascular rings (fig 3c) suggesting that this may be linked to changes in lumen diameter (fig 2e(ii) or differences in elastic properties of mutant blood vessels.

We next analysed for changes in contractile responses of pre-stretched, equilibrated vascular rings from Brn-3b KO and WT aortas by adding cumulative dose of known mediators of vascular contraction including phenylephrine (PE), prostaglandin analogue, U46619, or potassium chloride (KCl) [50-52]. Pooled data from independent aortas, taken from 6 WT and 6 Brn-3b KO mice, (Fig 4d) showed that vascular rings from WT aortas displayed dose-responsive increases in force of contraction following treatment, with PE causing the significant responses (i). However, contractile responses in Brn-3b KO aortas were considerably blunted following PE treatment, indicating that mutant aortas were unable to contract significantly. Similar effects were observed following treatment with U46619 (ii), and KCl (iii), which induced strong contraction of vascular rings from WT but significantly attenuated responses in Brn-3b KO aortas. These highly reproducible results from independent aortas suggests that pre-constriction of mutant aortas upon loss of Brn-3b may prevent subsequent contractile responses to PE, U46619 or KCl.

RNA sequencing analysis to identify genes altered in Brn-3b KO aortas:

To understand the molecular basis for such changes in Brn-3b KO aortas, RNA sequencing analysis was undertaken to identify genes that were differentially regulated upon loss of Brn-3b in the aorta. Following in-depth analysis of data using iDEP.91 software[53], principal

component analysis (PCA) identified one WT outlier (fig 4a) but K-means analysis of the top 2500 differentially regulated genes showed that the same gene clusters were identified when using all datasets (supplementary S-fig 1) or when the outlier was excluded (fig 5b). However, the outlier caused some skewing in subsequent analyses to identify up- and down regulated genes so was omitted for later analyses with selected genes validated in multiple, independent mRNA from WT or Brn-3b KO aortas.

The most consistent and significant gene expression changes between WT and mutant aortas were observed in 2 clusters, A and C (fig 5 & s-fig1b; s-table 1b). KEGG pathway analysis showed that genes in cluster A (844 genes; adjusted p-values <8.0e-0.3) were strongly associated with calcium signalling (adjP 3.4e-05) and muscle contraction (adjP 3.4e-05) (Fig 5) that directly affect vascular function while gene ontology (GO) analysis confirmed that genes within this cluster were mainly associated with the plasma membrane or ion channels in the S/ER and participated in biological processes including sarcomeric structures and ion transport, (s-table 1c and d). Since Ca^{2+} signalling genes are also implicated in controlling cardiac contractility and function[54-56], it is unsurprising that cardiac pathways including adrenergic signalling, cAMP signalling were also identified (s-table 1e). Interestingly, other affected genes within this cluster were linked to regulation of circadian entrainment (adjP 1.8e-03) and metabolic processes (adjP 5.3e-03), which can indirectly contribute to vascular dysfunction[57-59] (s-table 1). In contrast, genes in cluster C (521 genes; adjusted p-values <2.6 e-0.3) were mainly linked to regulation of VSMC contraction (adjP 3.6e-03) but also immune responses (adjP 2.6e-03), which can indirectly alter vascular function (supplementary table 1a) [10, 60, 61]. GO analysis also confirmed that cluster C genes were implicated in VSMC contraction and muscle development/ differentiation. Affected genes in cluster B (617 genes; adj p-values <7.5e-0.3) and D (542 genes; adj p-values <5.3e-0.3), were linked to

haematopoietic cell lineage and immune responses respectively but the sample-to-sample variation limited interpretation of this data.

Identification of up- & down-regulated genes

Gene Set Enrichment Analysis (GSEA) was next combined with KEGG pathway and GO analyses to identify how genes that were specifically up- or down-regulated in Brn-3b KO aortas affected key functional pathways that were linked to essential biological processes. Table 1a shows the largest number of upregulated genes in Brn-3b KO aortas (158 genes) were implicated in Ca^{2+} signalling and related pathways (cAMP signalling and β-adrenergic signalling) with significant normalisation enrichment scores (NES +1.51) while 93 genes (NES+1.45) were implicated in VSMC contraction. Supplementary table 1 (s-1) shows the list of genes within each cluster.

In support of essential findings for such differential gene expression, GO analyses of biological function and cellular component showed that genes within these groups encoded for ion channels (S/ER or plasma membrane) and regulatory proteins that were involved in biological and molecular processes such as Ca^{2+} signalling and muscle contractility (s-Table 2). Interestingly, genes affected by loss of Brn-3b were also implicated in human diseases since Jensen.disease pathway analysis (table 1c) showed that the most significant pathways affected by genes upregulated in Brn-3b KO aortas were hypertension (169 genes; NES+1.48) CAD (128 genes; NES+1.53).

Consistent with K-means cluster analysis, genes upregulated by loss of Brn-3b were also implicated in pathways that can indirectly affect vascular function including circadian rhythm and entrainment, (68 genes; NES+1.64); immune function (56 genes; NES+1.48 that included

IL-17 signalling, cytokine receptor interaction, haematopoietic cell lineage), and metabolic diseases (type II diabetes mellitus) (34 genes; NES+1.45), (Table1a and s-table 2a).

On the other hand, genes down-regulated in Brn-3b KO aortas were implicated in controlling VSMC function and related processes (table 1b), with 68 down-regulated genes (NES -1.64) linked to VSMC contraction; 40 genes (NES-1.75) associated with regulation of actin cytoskeleton and 33 genes (NES -1.79) linked to Apelin signalling pathway. Other down-regulated genes were linked to immune responses [37 reduced genes (NES -1.98) in chemokine signalling and 16 genes (NES -2.09) linked to IL-17 signalling, indicating complex but, as yet, unknown functions for Brn-3b in controlling vascular functions.

Differential expression of genes (DEG2) was next undertaken to identify the most significantly up- and down regulated genes, upon loss of Brn-3b. DESeq analyses showed that 59 genes were significantly upregulated and 74 genes down-regulated in Brn-3b KO aorta (fig 6a and b). Selected genes shown in table 2 a and b, highlight how genes that were up- or down regulated upon loss of Brn-3b affected key pathways involved in Ca^{2+} signalling and muscle contraction and is summarised in Fig 6c, which shows KEGG graph and proposed effects on calcium signalling pathways.

Notable Ca^{2+} signalling gene changes included up-regulation of CaV channels Cacn2d2, Cacna1d & Cacna1h but also RyR2 and Pln[62, 63] with reduced Atp2a1, S100e9 (Calgranulin A) and RyR1. Similarly, affected genes that control sarcomeric structure and muscle/VSMC contractility included up-regulation of Mmp12 (table 2a; fig 7a) as well as calcium-dependent phospholipase A2, (Pla2g2e) and atrial natriuretic peptide A (Nppa) with significant reduction of Eln (table 2b; fig 7a) and Actn3; Mylpf; Myl3. Other upregulated genes were linked to control

of circadian processes or metabolic function while many down regulated genes including Cxcr2, IL1 beta, Ccl12, Csf3r and Igsf9 that control immune responses suggesting other complex effects that may indirectly affect vascular function[64-67]. These results suggest that Brn-3b can regulate vascular contractility by activating or repressing genes that control Ca^{2+} signalling and muscle contractility either directly or indirectly via other processes such as inflammation or metabolic changes and deregulated expression upon loss of Brn-3b will contribute to abnormal vascular phenotype and contractile function (s-fig3).

Validation of selected genes:

Since loss of Brn-3b caused significant changes in Ca^{2+} signalling genes and S/ER function, these formed the basis for validation studies were focused on selected genes in these pathways. Fig 7b shows the results of qRT-PCR analysis of selected genes using cDNA from independent Brn-3b KO or WT aortas. Genes showing increased expression in Brn-3b KO aortas included the CaV channel Cacna1d and S/ER Ca^{2+} channel RyR2 but also PLN, which inhibits S/ER Ca^{2+} pump. Similar but non-significant increases were also seen for Cacnb2. On the other hand, genes showing marked reduction in Brn-3b KO aortas included ATP2a encoding SERCA1 Ca^{2+} pump and RyR1 but also genes encoding chaperone proteins, HspA8, HspH1 and DnaJa1, required for UPR in S/ER[19]. Such data suggest that loss of Brn-3b will result in increased intracellular Ca^{2+} but reduced S/ER Ca^{2+} reuptake, thereby increasing S/ER stress (supplementary fig 3). Reduction of chaperone proteins will also affect responses to S/ER stress and thereby contribute to vascular dysfunction in Brn-3b KO aortas. These results have led us to a proposed model whereby Brn-3b is an important regulator of key target genes that are required for maintaining normal vascular function. This may occur via different effects including regulation of structural components (e.g. elastin and collagen) or essential pathways that control Ca^{2+} signalling and S/ER stress responses. Therefore, loss of

Brn-3b intracellular levels will lead to increased intracellular Ca^{2+} and S/ER Ca^{2+} depletion but also increase ER stress and thereby lead to phenotypic switching and contractile dysfunction in VSMC's (fig 8).

Discussion:

VSMCs are essential for active regulation of arterial compliance and vascular tone in vessels, such as the aorta since changes in the phenotype and function of these cells can contribute significantly to the development of vascular dysfunction e.g. arterial stiffening & hypertension and increase the risk of CVD[8, 12-14 20, 68]. Yet, the chronic nature of such diseases means that such vascular damage often develop over relatively long periods but often remain asymptomatic and undetectable at early stages so the underlying molecular basis of such diseases have remained poorly understood, thereby frustrating attempts at early diagnosis and effective treatment to prevent irreversible damage[10, 12].

In this study, we showed for the first time that Brn-3b has essential but previously unknown roles in controlling vascular integrity and function by regulating the expression of genes that control Ca^{2+} signalling and contractile function as well as stress responses in VSMCs. While the first evidence pointing to Brn-3b expression in the vasculature arose from studies in stressed hearts showing that loss of Brn-3b caused extensive adverse remodeling around the coronary vasculature in male Brn-3b KO mice[29], the current studies has confirmed Brn-3b expression in the BV walls, with localisation in VSMC either in aortic sections or isolated primary VSMC cultures. The aorta provided a useful model to analyse Brn-3b expression in the vasculature but was also relevant because adverse changes in aortic elastance and compliance can affect cardiac contractility and contribute to abnormal contractile responses, previously reported in 2mth old Brn-3b KO mutants[29]. Moreover, the aorta provided a valuable source for isolating and analysing primary VSMC using standard in vitro culture.

The availability of the constitutive Brn-3b KO mutants also provided insights into the effects of loss of Brn-3b on aortic phenotype and function. The current studies were primarily

focused on male mutants because of previous data showing that male Brn-3b KO mice developed extensive coronary artery remodeling following chronic stress, which was not seen in female mutants[29]. As such, structural and histological abnormalities in aortas from male Brn-3b KO mutants were particularly interesting. For example, small but consistent coarctation defects in the descending aortas from 2mth old male Brn-3b KO mice were similar to abnormalities previously shown in heterozygote $Eln^{+/-}$ mice, where reduced elastin was strongly associated with hypertension[69, 70]. In line with this, histological staining of aortic sections, which showed disruption of elastin fibers seen in Brn-3b KO aortas were supported by ultrastructural changes observed in TEM images. Interestingly, RNA sequencing data showed that not only was Eln mRNA reduced in Brn-3b KO aortas, but mutant aortas also expressed higher levels of MMP12 elastase, which can contribute to disruption of elastin fibers seen in TEM images. TEM and immunostaining also confirmed increased collagen deposition in the thickened adventitial layers of Brn-3b KO aortas, which when combined with the observed reduction in lumen diameter can also contribute to arterial stiffening and contractile dysfunction[71]. This was indeed confirmed by wire myography with differences in IC100 in vascular rings from Brn-3b KO aortas potentially link to reduced lumen diameter and/or pre-contraction of vessels at baseline. In addition, abnormal responses in mutant BV was also confirmed following treatments known stimuli e.g. α-adrenergic agonist, PE, which elicited strong phasic and tonic contraction in WT VSMC via CaV channels[52, 72], caused markedly attenuated responses in vascular rings from Brn-3b KO aortas. Similarly, prostaglandin analogue U46619 and KCl induced strong contraction in WT VSMCs by raising intracellular Ca^{2+} levels via G-protein coupled receptors or via S/ER channels[49, 73 52, 74] but caused minimal responses in vascular rings from Brn-3b KO aortas. Importantly, vascular contractility induced by such treatment are mediated by effects of the Ca^{2+} signaling pathways[9,75]. This is particularly important in VSMC, where active contraction is tightly

regulated by changes in intracellular Ca^{2+}, with contraction controlled by expression and activity of specialised Ca^{2+} channels either in the plasma membrane or S/ER, which serve to increase intracellular Ca2+ and initiate vasoconstriction [13, 54, 76]. Conversely, repolarisation and relaxation depend upon rapid reduction of intracellular Ca^{2+} either by specialised pumps such as PMCA, which promote Ca^{2+} efflux or SERCA pumps, which facilitate Ca^{2+} reuptake into S/ER intracellular stores[10, 11, 74]. Therefore, abnormal contractile responses in vascular rings from Brn-3b KO aortas suggest deregulation of Ca^{2+} signaling pathways and in line with this, data from high throughput RNA sequencing showed that Ca^{2+} signaling genes were most significantly affected by loss of Brn-3b, suggesting that loss of Brn-3b can profoundly alter Ca^{2+} signalling pathways in VSMCs.

Indeed, K-means and KEGG pathway analysis showed that the largest numbers of genes affected by loss of Brn-3b more associated with Ca^{2+} signaling and vascular contraction and GO analysis confirmed that these genes encoded for proteins associated with plasma membrane or S/ER complexes and were involved in biological processes including Ca^{2+} and cation transport or muscle contraction[53]. Since Ca^{2+}signaling also controls contractility in cardiomyocytes, it is perhaps unsurprising that cardiac dysfunction and cardiomyopathies were also identified as affected pathways [77]. Similarly, GSEA and DEG analysis showed that the largest number of up-regulated genes (158) in Brn-3b KO aortas were implicated in Ca^{2+} signalling pathway while 93 upregulated and 68 down-regulated genes were associated with VSMC contraction e.g. actin cytoskeleton and Apelin signalling pathways, that controls vasodilation and are reduced in experimental hypertension models but also hypertensive patients[61, 78-80]. The link between loss of Brn-3b and hypertension was further reinforced by Jensen.Disease pathway of RNA sequencing data, which identified hypertension as the top disease pathway involving 169 upregulated genes in Brn-3b KO aortas associated while 120 affected genes were associated with coronary artery diseases (CAD) in humans. This was

particularly interesting because of existing GWAS data showing that SNPs within the Brn-3b genomic locus (chromosome 4q.31.2) were strongly associated with coronary heart disease (CHD), CAD and cerebrovascular accident (CVA)[40-45]. These data indicate that changes in Brn-3b expression in the vasculature can contribute to contractile dysfunction and CVD.

Subsequent validation studies that confirmed deregulation of Ca^{2+} signalling and S/ER pathways in independent Brn-3b KO aortas, were particularly important for identifying the underlying mechanisms that drive contractile abnormalities in Brn-3b KO mutants[17 81]. For instance, increased expression of genes encoding long-acting L-type CaV channels e.g. Cacna1d and Cacnb2, in Brn-3b KO aortas will raise intracellular Ca^{2+} and trigger contraction in VSMCs by facilitating Ca^{2+} efflux via plasma membrane. Therefore, such Ca^{2+} channels are often targeted by Ca^{2+} channel blockers used to treat patients with hypertension[63, 74, 81]. Despite reduced RyR1, increased expression of the RyR2 channels in Brn-3b KO aortas will also promote release of Ca^{2+} from the S/ER to increase intracellular Ca^{2+} while inducing localized transients that also contribute to vascular contraction[13, 16, 17]. As such, increases in these Ca^{2+} channel genes in Brn-3b KO VSMCs can promote abnormal vascular contractility both at baseline and in response to stimulus, as observed in myography[62, 82]. Moreover, sustained increases in intracellular Ca^{2+} may also contribute to phenotypic switching from contractile into proliferative VSMCs because raised intracellular Ca^{2+} can activate NFAT TF (via calcineurin pathway) to drive transcription of genes associated with cell proliferation[72].

On the other hand, loss of Brn-3b may also affect VSMC re-polarisation and relaxation in the aortas because although Atp2a1 was reduced and Atp2a2 levels remain unchanged, increased expression of the potent SERCA pump inhibitor, Pln, will prevent Ca^{2+} reuptake into the S/ER. Inhibition of SERCA activity combined with enhanced Ca^{2+} release (via increased Ryr2) will lead to S/ER Ca^{2+} depletion and contribute to ER stress and UPR[24].

However, reduction in chaperone proteins such as the known Brn-3b target gene Hsp27 (HspB1)[34], HspA8, HspH1 and DnaJa1, will prevent adaptive UPR and thereby trigger phenotypic switching from contractile into proliferative VSMCs[20, 25].

These results suggest that Brn-3b is important for regulating genes that control Ca^{2+} signalling and VSMC contraction in arterial blood vessels and loss of Brn-3b will contribute to contractile dysfunction, which precedes the development of vascular dysfunction including hypertension and subsequent progression to CAD. Therefore, elucidating the effects of loss of Brn-3b and its target genes could provide insight into the molecular basis of early vascular changes and subsequent development vascular dysfunction /damage[83].

Since this study was undertaken using the constitutive Brn-3b KO mutants, it is noteworthy that loss of Brn-3b caused deregulation of genes that are implicated in regulating immune responses, circadian entrainment and metabolic processes, which can indirectly affect vascular function. Although future studies using tissue-specific mutants can help to determine direct and indirect effects of loss of Brn-3b in the vasculature, changes in different subsets of genes are nonetheless interesting and relevant in view of previous studies showing Brn-3b expression and effects of its loss on relevant tissues. For instance, previous studies showing metabolic dysfunction in Brn-3b KO mutants (hyperglycaemia, insulin resistance and increased visceral WAT deposits[28-30]), means that deregulation of metabolic genes in Brn-3b KO aortas was unsurprising. However, despite careful attempts to remove all excess tissues around the aortas used for RNA sequencing, at this stage it is unclear if such genes are affected by metabolic changes in the mutant aortas or are link to residual PVAT. Nevertheless, these observations are also interesting because adipose tissues can exerts profound endocrine effects on BV wall by producing vasoactive modulators such as

adipokines and cytokines[84-86]. Indeed, common metabolic dysfunction such as obesity and diabetes are commonly linked to increased risk factors of damage to coronary and systemic circulation and subsequent CVD[10]. Since Brn-3b KO PVAT display significant increases in WAT content which produces pro-inflammatory adipokines and cytokines will affect the inflammatory milieu by and alter VSMC phenotype and function[60, 84, 87, 88]. In line with this, TEM images showing increased infiltration of local sites into the PVAT surrounding Brn-3b KO aortas was confirmed by RNA sequencing data showing significant changes in involved in pro-inflammatory pathways including IL-17 signalling and cytokine-cytokine receptor interaction pathways, which are implicated in development of vascular dysfunction and CVDs including hypertension and atherosclerosis[2]. Although the link between loss of Brn-3b and deregulated immune responses are still to be determined, Brn-3b is expressed in immune cells e.g. monocytes[89, 90], T cells and PBMCs[91, 92], so it will be interesting to determine if inflammatory effects in Brn-3b KO tissues cause direct or indirect effects on vascular function and transition to vascular diseases[58]. Furthermore, the implications and effects of upregulation of genes that control circadian processes changes in Brn-3b KO aortas remain unknown but since disruption of the circadian rhythm is commonly associated with ageing and risk of vascular, cardiac and metabolic diseases[58, 93, 94], these mutants model could provide some interesting insight into the mechanisms linking such conditions.

In conclusion, the Brn-3b TF represents a novel and important regulator of genes that control Ca^{2+} in VSMCs and thereby regulate vascular contractility and function. Since Ca^{2+} signaling pathways are pivotal for controlling multiple cellular functions in different cell types, such regulation by Brn-3b could have wider implications in understanding how this factor controls gene expression and cell fate in other cellular contexts also. Loss of Brn-3b also appears to be linked to structural and functional changes in the aortas and was strongly linked to

hypertension and coronary artery disease either in Jensen.Disease pathway analysis or GWAS data showing that SNPs in Brn-3b genomic region (chromosome 4q31) were associated with increased risk of hypertension and CHD[40-42]. Therefore, these novel findings may provide insight into if/how reduction or loss of Brn-3b may drive early vascular changes during early stages of vascular dysfunction and progression to disease. Finally, deregulation of genes involved in other key processes including immune function, circadian regulation and metabolic processes in Brn-3b KO aortas points to complex but as yet unknown mechanisms by which this regulator may indirectly affect vascular function.

Acknowledgements:

We express our sincere gratitude to Dr Caroline Pellet-Many for advice and assistance with culturing VSMC from rat and mouse aortas and Prof Mike Duchen for support with the calcium imaging. Aortic velocity measurements were done using ultrasound analysis carried out by Dr Lauren Maskell and Dr Daniel Stuckey.

Source of funding: This research was funded by the BHF (PG/16/73/32364 and FS/17/8/32664).

Disclosures: There is no conflict of interest associated with any authors in this study.

Authors' contribution:

Vaishaali Yogendran and Laura Mele undertook most of the experimental studies and analysis and were involved in providing feedback on the manuscript. Oleksandra Prysyazhna carried out the myography analysis, provided data for this study and provided feedback on the manuscript. Vishwanie S. Budhram-Mahadeo is the lead author involved in conception

and design of the project as well as obtaining funding for undertaking the research. VB-M also helped to plan and supervised experimental studies, undertook analysis of the RNA sequencing data and prepared the manuscript for publication.

References:

1. Witteman JC, Kannel WB, Wolf PA, Grobbee DE, Hofman A, D'Agostino RB, Cobb JC. Aortic calcified plaques and cardiovascular disease (the Framingham Study). *Am J Cardiol* 1990;**66**:1060-1064.
2. Frostegard J. Immunity, atherosclerosis and cardiovascular disease. *BMC Med* 2013;**11**:117.
3. Bonarjee VVS. Arterial Stiffness: A Prognostic Marker in Coronary Heart Disease. Available Methods and Clinical Application. *Front Cardiovasc Med* 2018;**5**:64.
4. Kamberi LS, Gorani DR, Hoxha TF, Zahiti BF. Aortic Compliance and Stiffness Among Severe Longstanding Hypertensive and Non-hypertensive. *Acta Inform Med* 2013;**21**:12-15.
5. Boutouyrie P, Tropeano AI, Asmar R, Gautier I, Benetos A, Lacolley P, Laurent S. Aortic stiffness is an independent predictor of primary coronary events in hypertensive patients: a longitudinal study. *Hypertension* 2002;**39**:10-15.
6. Laurent S, Boutouyrie P, Asmar R, Gautier I, Laloux B, Guize L, Ducimetiere P, Benetos A. Aortic stiffness is an independent predictor of all-cause and cardiovascular mortality in hypertensive patients. *Hypertension* 2001;**37**:1236-1241.
7. Zieman SJ, Melenovsky V, Kass DA. Mechanisms, pathophysiology, and therapy of arterial stiffness. *Arterioscler Thromb Vasc Biol* 2005;**25**:932-943.
8. Gasser TC. Aorta. In: Ohayon YPaJ, ed. Biomechanics of Living Organs: Elsevier Inc, 2017:169-191.
9. Shanahan CM, Weissberg PL. Smooth muscle cell heterogeneity: patterns of gene expression in vascular smooth muscle cells in vitro and in vivo. *Arterioscler Thromb Vasc Biol* 1998;**18**:333-338.
10. Lacolley P, Regnault V, Segers P, Laurent S. Vascular Smooth Muscle Cells and Arterial Stiffening: Relevance in Development, Aging, and Disease. *Physiol Rev* 2017;**97**:1555-1617.
11. Iyemere VP, Proudfoot D, Weissberg PL, Shanahan CM. Vascular smooth muscle cell phenotypic plasticity and the regulation of vascular calcification. *J Intern Med* 2006;**260**:192-210.
12. Wilson DP. Vascular Smooth Muscle Structure and Function. In: Fitridge R, Thompson M, eds. Mechanisms of Vascular Disease: A Reference Book for Vascular Specialists. Adelaide (AU), 2011.
13. Hill-Eubanks DC, Werner ME, Heppner TJ, Nelson MT. Calcium signaling in smooth muscle. *Cold Spring Harb Perspect Biol* 2011;**3**:a004549.
14. Lipskaia LL, I., Bobe R. and Hajjar R. Calcium Cycling in Synthetic and Contractile Phasic or Tonic Vascular Smooth Muscle Cells. *Current Basic and Pathological Approaches to the Function of Muscle Cells and Tissues* 2012;**Open access peer-reviewed chapter**.
15. Liu Z, Khalil RA. Evolving mechanisms of vascular smooth muscle contraction highlight key targets in vascular disease. *Biochem Pharmacol* 2018;**153**:91-122.
16. Jaggar JH, Porter VA, Lederer WJ, Nelson MT. Calcium sparks in smooth muscle. *Am J Physiol Cell Physiol* 2000;**278**:C235-256.
17. Golovina VA, Blaustein MP. Spatially and functionally distinct Ca2+ stores in sarcoplasmic and endoplasmic reticulum. *Science* 1997;**275**:1643-1648.
18. Wray S, Burdyga T. Sarcoplasmic reticulum function in smooth muscle. *Physiol Rev* 2010;**90**:113-178.
19. Wu KD, Bungard D, Lytton J. Regulation of SERCA Ca2+ pump expression by cytoplasmic Ca2+ in vascular smooth muscle cells. *Am J Physiol Cell Physiol* 2001;**280**:C843-851.

20. House SJ, Potier M, Bisaillon J, Singer HA, Trebak M. The non-excitable smooth muscle: calcium signaling and phenotypic switching during vascular disease. *Pflugers Arch* 2008;**456**:769-785.
21. Clarke MC, Figg N, Maguire JJ, Davenport AP, Goddard M, Littlewood TD, Bennett MR. Apoptosis of vascular smooth muscle cells induces features of plaque vulnerability in atherosclerosis. *Nat Med* 2006;**12**:1075-1080.
22. Regan CP, Adam PJ, Madsen CS, Owens GK. Molecular mechanisms of decreased smooth muscle differentiation marker expression after vascular injury. *J Clin Invest* 2000;**106**:1139-1147.
23. Kapustin AN, Shanahan CM. Emerging roles for vascular smooth muscle cell exosomes in calcification and coagulation. *J Physiol* 2016.
24. Liang B, Wang S, Wang Q, Zhang W, Viollet B, Zhu Y, Zou MH. Aberrant endoplasmic reticulum stress in vascular smooth muscle increases vascular contractility and blood pressure in mice deficient of AMP-activated protein kinase-alpha2 in vivo. *Arterioscler Thromb Vasc Biol* 2013;**33**:595-604.
25. Tabas I. The role of endoplasmic reticulum stress in the progression of atherosclerosis. *Circ Res* 2010;**107**:839-850.
26. Kadonaga JT. Eukaryotic transcription: an interlaced network of transcription factors and chromatin-modifying machines
4. *Cell* 1998;**92**:307-313.
27. Chakraborty RPC, Jui M. Dave, Allison C. Ostriker, Daniel M. Greif, Eva M. Rzucidlo and Kathleen A. Martin, . Targeting smooth muscle cell phenotypic switching in vascular disease. *JVSeVascular Science* 2021;**preprint**:1-16.
28. Budhram-Mahadeo VS, Solomons MR, Mahadeo-Heads EAO. Linking metabolic dysfunction with cardiovascular diseases: Brn-3b/POU4F2 transcription factor in cardiometabolic tissues in health and disease. *Cell Death Dis* 2021;**12**:267.
29. Mele L, Maskell LJ, Stuckey DJ, Clark JE, Heads RJ, Budhram-Mahadeo VS. The POU4F2/Brn-3b transcription factor is required for the hypertrophic response to angiotensin II in the heart. *Cell Death Dis* 2019;**10**:621.
30. Bitsi S, Ali H, Maskell L, Ounzain S, Mohamed-Ali V, Budhram-Mahadeo VS. Profound hyperglycemia in knockout mutant mice identifies novel function for POU4F2/Brn-3b in regulating metabolic processes. *Am J Physiol Endocrinol Metab* 2016;**310**:E303-312.
31. Budhram-Mahadeo V, Fujita R, Bitsi S, Sicard P, Heads R. Co-expression of POU4F2/Brn-3b with p53 may be important for controlling expression of pro-apoptotic genes in cardiomyocytes following ischaemic/hypoxic insults. *Cell Death Dis* 2014;**5**:e1503.
32. Budhram-Mahadeo V, Morris PJ, Lakin ND, Theil T, Ching GY, Lillycrop KA, Moroy T, Liem RK, Latchman DS. Activation of the alpha-internexin promoter by the Brn-3a transcription factor is dependent on the N-terminal region of the protein. *J Biol Chem* 1995;**270**:2853-2858.
33. Ounzain S, Bowen S, Patel C, Fujita R, Heads RJ, Budhram-Mahadeo VS. Proliferation-associated POU4F2/Brn-3b transcription factor expression is regulated by oestrogen through ERalpha and growth factors via MAPK pathway. *Breast Cancer Res* 2011;**13**:R5.
34. Lee SA, Ndisang D, Patel C, Dennis JH, Faulkes DJ, D'Arrigo C, Samady L, Farooqui-Kabir S, Heads RJ, Latchman DS, Budhram-Mahadeo VS. Expression of the Brn-3b transcription factor correlates with expression of HSP-27 in breast cancer biopsies and is required for maximal activation of the HSP-27 promoter. *Cancer Res* 2005;**65**:3072-3080.
35. Cho JH, Mu X, Wang SW, Klein WH. Retinal ganglion cell death and optic nerve degeneration by genetic ablation in adult mice. *Exp Eye Res* 2009;**88**:542-552.
36. Mu X, Beremand PD, Zhao S, Pershad R, Sun H, Scarpa A, Liang S, Thomas TL, Klein WH. Discrete gene sets depend on POU domain transcription factor Brn3b/Brn-3.2/POU4f2 for their expression in the mouse embryonic retina. *Development* 2004;**131**:1197-1210.
37. Budhram-Mahadeo VS, Irshad S, Bowen S, Lee SA, Samady L, Tonini GP, Latchman DS. Proliferation-associated Brn-3b transcription factor can activate cyclin D1 expression in neuroblastoma and breast cancer cells. *Oncogene* 2008;**27**:145-154.

38. Samady L, Dennis J, Budhram-Mahadeo V, Latchman DS. Activation of CDK4 gene expression in human breast cancer cells by the Brn-3b POU family transcription factor. *Cancer Biol Ther* 2004;**3**:317-323.
39. Maskell LJ, Qamar K, Babakr AA, Hawkins TA, Heads RJ, Budhram-Mahadeo VS. Essential but partially redundant roles for POU4F1/Brn-3a and POU4F2/Brn-3b transcription factors in the developing heart. *Cell Death Dis* 2017;**8**:e2861.
40. Howson JMM, Zhao W, Barnes DR, Ho WK, Young R, Paul DS, Waite LL, Freitag DF, Fauman EB, Salfati EL, Sun BB, Eicher JD, Johnson AD, Sheu WHH, Nielsen SF, Lin WY, Surendran P, Malarstig A, Wilk JB, Tybjaerg-Hansen A, Rasmussen KL, Kamstrup PR, Deloukas P, Erdmann J, Kathiresan S, Samani NJ, Schunkert H, Watkins H, CardioGramplusC4D, Do R, Rader DJ, Johnson JA, Hazen SL, Quyyumi AA, Spertus JA, Pepine CJ, Franceschini N, Justice A, Reiner AP, Buyske S, Hindorff LA, Carty CL, North KE, Kooperberg C, Boerwinkle E, Young K, Graff M, Peters U, Absher D, Hsiung CA, Lee WJ, Taylor KD, Chen YH, Lee IT, Guo X, Chung RH, Hung YJ, Rotter JI, Juang JJ, Quertermous T, Wang TD, Rasheed A, Frossard P, Alam DS, Majumder AAS, Di Angelantonio E, Chowdhury R, Epic CVD, Chen YI, Nordestgaard BG, Assimes TL, Danesh J, Butterworth AS, Saleheen D. Fifteen new risk loci for coronary artery disease highlight arterial-wall-specific mechanisms. *Nat Genet* 2017;**49**:1113-1119.
41. Nikpay M, Goel A, Won HH, Hall LM, Willenborg C, Kanoni S, Saleheen D, Kyriakou T, Nelson CP, Hopewell JC, Webb TR, Zeng L, Dehghan A, Alver M, Armasu SM, Auro K, Bjonnes A, Chasman DI, Chen S, Ford I, Franceschini N, Gieger C, Grace C, Gustafsson S, Huang J, Hwang SJ, Kim YK, Kleber ME, Lau KW, Lu X, Lu Y, Lyytikainen LP, Mihailov E, Morrison AC, Pervjakova N, Qu L, Rose LM, Salfati E, Saxena R, Scholz M, Smith AV, Tikkanen E, Uitterlinden A, Yang X, Zhang W, Zhao W, de Andrade M, de Vries PS, van Zuydam NR, Anand SS, Bertram L, Beutner F, Dedoussis G, Frossard P, Gauguier D, Goodall AH, Gottesman O, Haber M, Han BG, Huang J, Jalilzadeh S, Kessler T, Konig IR, Lannfelt L, Lieb W, Lind L, Lindgren CM, Lokki ML, Magnusson PK, Mallick NH, Mehra N, Meitinger T, Memon FU, Morris AP, Nieminen MS, Pedersen NL, Peters A, Rallidis LS, Rasheed A, Samuel M, Shah SH, Sinisalo J, Stirrups KE, Trompet S, Wang L, Zaman KS, Ardissino D, Boerwinkle E, Borecki IB, Bottinger EP, Buring JE, Chambers JC, Collins R, Cupples LA, Danesh J, Demuth I, Elosua R, Epstein SE, Esko T, Feitosa MF, Franco OH, Franzosi MG, Granger CB, Gu D, Gudnason V, Hall AS, Hamsten A, Harris TB, Hazen SL, Hengstenberg C, Hofman A, Ingelsson E, Iribarren C, Jukema JW, Karhunen PJ, Kim BJ, Kooner JS, Kullo IJ, Lehtimaki T, Loos RJF, Melander O, Metspalu A, Marz W, Palmer CN, Perola M, Quertermous T, Rader DJ, Ridker PM, Ripatti S, Roberts R, Salomaa V, Sanghera DK, Schwartz SM, Seedorf U, Stewart AF, Stott DJ, Thiery J, Zalloua PA, O'Donnell CJ, Reilly MP, Assimes TL, Thompson JR, Erdmann J, Clarke R, Watkins H, Kathiresan S, McPherson R, Deloukas P, Schunkert H, Samani NJ, Farrall M. A comprehensive 1,000 Genomes-based genome-wide association meta-analysis of coronary artery disease. *Nat Genet* 2015;**47**:1121-1130.
42. Shah S, Henry A, Roselli C, Lin H, Sveinbjornsson G, Fatemifar G, Hedman AK, Wilk JB, Morley MP, Chaffin MD, Helgadottir A, Verweij N, Dehghan A, Almgren P, Andersson C, Aragam KG, Arnlov J, Backman JD, Biggs ML, Bloom HL, Brandimarto J, Brown MR, Buckbinder L, Carey DJ, Chasman DI, Chen X, Chen X, Chung J, Chutkow W, Cook JP, Delgado GE, Denaxas S, Doney AS, Dorr M, Dudley SC, Dunn ME, Engstrom G, Esko T, Felix SB, Finan C, Ford I, Ghanbari M, Ghasemi S, Giedraitis V, Giulianini F, Gottdiener JS, Gross S, Guethbjartsson DF, Gutmann R, Haggerty CM, van der Harst P, Hyde CL, Ingelsson E, Jukema JW, Kavousi M, Khaw KT, Kleber ME, Kober L, Koekemoer A, Langenberg C, Lind L, Lindgren CM, London B, Lotta LA, Lovering RC, Luan J, Magnusson P, Mahajan A, Margulies KB, Marz W, Melander O, Mordi IR, Morgan T, Morris AD, Morris AP, Morrison AC, Nagle MW, Nelson CP, Niessner A, Niiranen T, O'Donoghue ML, Owens AT, Palmer CNA, Parry HM, Perola M, Portilla-Fernandez E, Psaty BM, Regeneron Genetics C, Rice KM, Ridker PM, Romaine SPR, Rotter JI, Salo P, Salomaa V, van Setten J, Shalaby AA, Smelser DT, Smith NL, Stender S, Stott DJ, Svensson P, Tammesoo ML, Taylor KD, Teder-Laving M, Teumer A, Thorgeirsson G, Thorsteinsdottir U, Torp-Pedersen C, Trompet S, Tyl B, Uitterlinden AG, Veluchamy A, Volker U, Voors AA, Wang X, Wareham NJ, Waterworth D, Weeke PE, Weiss

R, Wiggins KL, Xing H, Yerges-Armstrong LM, Yu B, Zannad F, Zhao JH, Hemingway H, Samani NJ, McMurray JJV, Yang J, Visscher PM, Newton-Cheh C, Malarstig A, Holm H, Lubitz SA, Sattar N, Holmes MV, Cappola TP, Asselbergs FW, Hingorani AD, Kuchenbaecker K, Ellinor PT, Lang CC, Stefansson K, Smith JG, Vasan RS, Swerdlow DI, Lumbers RT. Genome-wide association and Mendelian randomisation analysis provide insights into the pathogenesis of heart failure. *Nat Commun* 2020;**11**:163.

43. Erdmann J, Kessler T, Munoz Venegas L, Schunkert H. A decade of genome-wide association studies for coronary artery disease: the challenges ahead. *Cardiovasc Res* 2018;**114**:1241-1257.
44. Klarin D, Zhu QM, Emdin CA, Chaffin M, Horner S, McMillan BJ, Leed A, Weale ME, Spencer CCA, Aguet F, Segre AV, Ardlie KG, Khera AV, Kaushik VK, Natarajan P, Consortium CAD, Kathiresan S. Genetic analysis in UK Biobank links insulin resistance and transendothelial migration pathways to coronary artery disease. *Nat Genet* 2017;**49**:1392-1397.
45. Verweij N, Eppinga RN, Hagemeijer Y, van der Harst P. Identification of 15 novel risk loci for coronary artery disease and genetic risk of recurrent events, atrial fibrillation and heart failure. *Sci Rep* 2017;**7**:2761.
46. Mekahli D, Bultynck G, Parys JB, De Smedt H, Missiaen L. Endoplasmic-reticulum calcium depletion and disease. *Cold Spring Harb Perspect Biol* 2011;**3**.
47. Dritsoula A, Papaioannou I, Guerra SG, Fonseca C, Martin J, Herrick AL, Abraham DJ, Denton CP, Ponticos M. Molecular Basis for Dysregulated Activation of NKX2-5 in the Vascular Remodeling of Systemic Sclerosis. *Arthritis Rheumatol* 2018;**70**:920-931.
48. Jin L, Lipinski A, Conklin DJ. A Simple Method for Normalization of Aortic Contractility. *J Vasc Res* 2018;**55**:177-186.
49. Feelisch M, Akaike T, Griffiths K, Ida T, Prysyazhna O, Goodwin JJ, Gollop ND, Fernandez BO, Minnion M, Cortese-Krott MM, Borgognone A, Hayes RM, Eaton P, Frenneaux MP, Madhani M. Long-lasting blood pressure lowering effects of nitrite are NO-independent and mediated by hydrogen peroxide, persulfides, and oxidation of protein kinase G1alpha redox signalling. *Cardiovasc Res* 2020;**116**:51-62.
50. Williams SP, Dorn GW, 2nd, Rapoport RM. Prostaglandin I2 mediates contraction and relaxation of vascular smooth muscle. *Am J Physiol* 1994;**267**:H796-803.
51. Cogolludo A, Moreno L, Bosca L, Tamargo J, Perez-Vizcaino F. Thromboxane A2-induced inhibition of voltage-gated K+ channels and pulmonary vasoconstriction: role of protein kinase Czeta. *Circ Res* 2003;**93**:656-663.
52. Ratz PH, Berg KM, Urban NH, Miner AS. Regulation of smooth muscle calcium sensitivity: KCl as a calcium-sensitizing stimulus. *Am J Physiol Cell Physiol* 2005;**288**:C769-783.
53. Ge SX, Son EW, Yao R. iDEP: an integrated web application for differential expression and pathway analysis of RNA-Seq data. *BMC Bioinformatics* 2018;**19**:534.
54. Alonso-Carbajo L, Kecskes M, Jacobs G, Pironet A, Syam N, Talavera K, Vennekens R. Muscling in on TRP channels in vascular smooth muscle cells and cardiomyocytes. *Cell Calcium* 2017;**66**:48-61.
55. Tian CJ, Zhang JH, Liu J, Ma Z, Zhen Z. Ryanodine receptor and immune-related molecules in diabetic cardiomyopathy. *ESC Heart Fail* 2021;**8**:2637-2646.
56. Louch WE, Koivumaki JT, Tavi P. Calcium signalling in developing cardiomyocytes: implications for model systems and disease. *J Physiol* 2015;**593**:1047-1063.
57. Maury E, Ramsey KM, Bass J. Circadian rhythms and metabolic syndrome: from experimental genetics to human disease. *Circ Res* 2010;**106**:447-462.
58. Gao P, Gao P, Choi M, Chegireddy K, Slivano OJ, Zhao J, Zhang W, Long X. Transcriptome analysis of mouse aortae reveals multiple novel pathways regulated by aging. *Aging (Albany NY)* 2020;**12**:15603-15623.
59. Grundy SM, Benjamin IJ, Burke GL, Chait A, Eckel RH, Howard BV, Mitch W, Smith SC, Jr., Sowers JR. Diabetes and cardiovascular disease: a statement for healthcare professionals from the American Heart Association. *Circulation* 1999;**100**:1134-1146.
60. Hotamisligil GS. Inflammation and metabolic disorders. *Nature* 2006;**444**:860-867.
61. Wysocka MB, Pietraszek-Gremplewicz K, Nowak D. The Role of Apelin in Cardiovascular Diseases, Obesity and Cancer. *Front Physiol* 2018;**9**:557.

62. Oloizia B, Paul RJ. Ca2+ clearance and contractility in vascular smooth muscle: evidence from gene-altered murine models. *J Mol Cell Cardiol* 2008;**45**:347-362.
63. Ghosh D, Syed AU, Prada MP, Nystoriak MA, Santana LF, Nieves-Cintron M, Navedo MF. Calcium Channels in Vascular Smooth Muscle. *Adv Pharmacol* 2017;**78**:49-87.
64. Stojanovic SD, Fuchs M, Kunz M, Xiao K, Just A, Pich A, Bauersachs J, Fiedler J, Sedding D, Thum T. Inflammatory Drivers of Cardiovascular Disease: Molecular Characterization of Senescent Coronary Vascular Smooth Muscle Cells. *Front Physiol* 2020;**11**:520.
65. Cuneo AA, Autieri MV. Expression and function of anti-inflammatory interleukins: the other side of the vascular response to injury. *Curr Vasc Pharmacol* 2009;**7**:267-276.
66. Schultz K, Murthy V, Tatro JB, Beasley D. Endogenous interleukin-1 alpha promotes a proliferative and proinflammatory phenotype in human vascular smooth muscle cells. *Am J Physiol Heart Circ Physiol* 2007;**292**:H2927-2934.
67. Seshiah PN, Kereiakes DJ, Vasudevan SS, Lopes N, Su BY, Flavahan NA, Goldschmidt-Clermont PJ. Activated monocytes induce smooth muscle cell death: role of macrophage colony-stimulating factor and cell contact. *Circulation* 2002;**105**:174-180.
68. Owens GK, Kumar MS, Wamhoff BR. Molecular regulation of vascular smooth muscle cell differentiation in development and disease. *Physiol Rev* 2004;**84**:767-801.
69. Owens EA, Jie L, Reyes BAS, Van Bockstaele EJ, Osei-Owusu P. Elastin insufficiency causes hypertension, structural defects and abnormal remodeling of renal vascular signaling. *Kidney Int* 2017;**92**:1100-1118.
70. Kenny D, Polson JW, Martin RP, Paton JF, Wolf AR. Hypertension and coarctation of the aorta: an inevitable consequence of developmental pathophysiology. *Hypertens Res* 2011;**34**:543-547.
71. Yasmin, O'Shaughnessy KM. Genetics of arterial structure and function: towards new biomarkers for aortic stiffness? *Clin Sci (Lond)* 2008;**114**:661-677.
72. Pang X, Sun NL. Calcineurin-NFAT signaling is involved in phenylephrine-induced vascular smooth muscle cell proliferation. *Acta Pharmacol Sin* 2009;**30**:537-544.
73. McKenzie C, MacDonald A, Shaw AM. Mechanisms of U46619-induced contraction of rat pulmonary arteries in the presence and absence of the endothelium. *Br J Pharmacol* 2009;**157**:581-596.
74. Amberg GC, Navedo MF. Calcium dynamics in vascular smooth muscle. *Microcirculation* 2013;**20**:281-289.
75. Brozovich FV, Nicholson CJ, Degen CV, Gao YZ, Aggarwal M, Morgan KG. Mechanisms of Vascular Smooth Muscle Contraction and the Basis for Pharmacologic Treatment of Smooth Muscle Disorders. *Pharmacol Rev* 2016;**68**:476-532.
76. House RL, Cassady JP, Eisen EJ, Eling TE, Collins JB, Grissom SF, Odle J. Functional genomic characterization of delipidation elicited by trans-10, cis-12-conjugated linoleic acid (t10c12-CLA) in a polygenic obese line of mice. *Physiol Genomics* 2005;**21**:351-361.
77. Fearnley CJ, Roderick HL, Bootman MD. Calcium signaling in cardiac myocytes. *Cold Spring Harb Perspect Biol* 2011;**3**:a004242.
78. Japp AG, Cruden NL, Barnes G, van Gemeren N, Mathews J, Adamson J, Johnston NR, Denvir MA, Megson IL, Flapan AD, Newby DE. Acute cardiovascular effects of apelin in humans: potential role in patients with chronic heart failure. *Circulation* 2010;**121**:1818-1827.
79. Kleinz MJ, Davenport AP. Immunocytochemical localization of the endogenous vasoactive peptide apelin to human vascular and endocardial endothelial cells. *Regul Pept* 2004;**118**:119-125.
80. Kuba K, Zhang L, Imai Y, Arab S, Chen M, Maekawa Y, Leschnik M, Leibbrandt A, Markovic M, Schwaighofer J, Beetz N, Musialek R, Neely GG, Komnenovic V, Kolm U, Metzler B, Ricci R, Hara H, Meixner A, Nghiem M, Chen X, Dawood F, Wong KM, Sarao R, Cukerman E, Kimura A, Hein L, Thalhammer J, Liu PP, Penninger JM. Impaired heart contractility in Apelin gene-deficient mice associated with aging and pressure overload. *Circ Res* 2007;**101**:e32-42.
81. Fransen P, Van Hove CE, Leloup AJ, Martinet W, De Meyer GR, Lemmens K, Bult H, Schrijvers DM. Dissecting out the complex Ca2+-mediated phenylephrine-induced contractions of mouse aortic segments. *PLoS One* 2015;**10**:e0121634.

82. Weissberg PL, Cary NR, Shanahan CM. Gene expression and vascular smooth muscle cell phenotype. *Blood Press Suppl* 1995;**2**:68-73.
83. Younes M, Lechago J, Chakraborty S, Ostrowski M, Bridges M, Meriano F, Solcher D, Barroso A, Whitman D, Schwartz J, Johnson C, Schmulen AC, Verm R, Balsaver A, Carlson N, Ertant A. Relationship between dysplasia, p53 protein accumulation, DNA ploidy, and Glut1 overexpression in Barrett metaplasia. *Scand J Gastroenterol* 2000;**35**:131-137.
84. Soltis EE, Cassis LA. Influence of perivascular adipose tissue on rat aortic smooth muscle responsiveness. *Clin Exp Hypertens A* 1991;**13**:277-296.
85. Montani JP, Carroll JF, Dwyer TM, Antic V, Yang Z, Dulloo AG. Ectopic fat storage in heart, blood vessels and kidneys in the pathogenesis of cardiovascular diseases. *Int J Obes Relat Metab Disord* 2004;**28 Suppl 4**:S58-65.
86. Lehman SJ, Massaro JM, Schlett CL, O'Donnell CJ, Hoffmann U, Fox CS. Peri-aortic fat, cardiovascular disease risk factors, and aortic calcification: the Framingham Heart Study. *Atherosclerosis* 2010;**210**:656-661.
87. Chang L, Garcia-Barrio MT, Chen YE. Perivascular Adipose Tissue Regulates Vascular Function by Targeting Vascular Smooth Muscle Cells. *Arterioscler Thromb Vasc Biol* 2020;**40**:1094-1109.
88. Horimatsu T, Kim HW, Weintraub NL. The Role of Perivascular Adipose Tissue in Non-atherosclerotic Vascular Disease. *Front Physiol* 2017;**8**:969.
89. Neme A, Nurminen V, Seuter S, Carlberg C. The vitamin D-dependent transcriptome of human monocytes. *J Steroid Biochem Mol Biol* 2016;**164**:180-187.
90. Nurminen V, Seuter S, Carlberg C. Primary Vitamin D Target Genes of Human Monocytes. *Front Physiol* 2019;**10**:194.
91. Bhargava AK, Li Z, Weissman SM. Differential expression of four members of the POU family of proteins in activated and phorbol 12-myristate 13-acetate-treated Jurkat T cells
1. *Proc Natl Acad Sci U S A* 1993;**90**:10260-10264.
92. Ripley BJ, Rahman MA, Isenberg DA, Latchman DS. Elevated expression of the Brn-3a and Brn-3b transcription factors in systemic lupus erythematosus correlates with antibodies to Brn-3 and overexpression of Hsp90. *Arthritis Rheum* 2005;**52**:1171-1179.
93. Takeda N, Maemura K. Circadian clock and vascular disease. *Hypertens Res* 2010;**33**:645-651.
94. Desvergne B, Michalik L, Wahli W. Transcriptional regulation of metabolism. *Physiol Rev* 2006;**86**:465-514.

Figure legends:

Figure 1: Brn-3b expression in aortic protein extracts and VSMC cultures.

(a) WB showing Brn-3b protein in WT mouse aortic extracts, compared with Brn-3b KO aortic extracts (negative control). β–tubulin blots indicate variation in protein loading. (b) Representative images of immunostained WT aortic sections showing co-localisation of Brn-3b (brown) with VSMC marker, αSMA (magenta). Negative control = 2nd Ab and α-SMA. (c) Representative immunofluorescent images of aortic VSMCs from WT moice (top panel) or Brn-3b KO mice, co-stained with Brn-3b (green) and α–SMA (red). DAPI mount indicates cell nuclei (blue).

Figure 2a-b: Histological changes in Brn-3b KO aorta compared with WT

Representative images of intact aortas taken from WT or Brn-3b KO mice, after staining for oil red. Images shown at X5 magnification with boxed areas expanded to highlight narrowing/constriction in Brn-3b KO aortas and corresponding WT aortas.

(a) H&E staining of longitudinal aortic sections from WT (i) or Brn-3b KO mice (ii). X20 magnification of selected areas shows increased adventitial thickness highlighted by dotted lines (arrows indicate specific areas of thickening in KO aortas; * highlights increased WAT deposition). L = lumen.

(b)Representative images showing Masson's trichrome staining of longitudinal aortic sections from either (i) WT or (ii) Brn-3b KO mice which highlights the increases in TA thickness (rounded brackets) and areas with elastin disruption in Brn-3b KO aortas (*). Red staining represent cytoplasm staining; dark purple/black indicates cell nuclei; blue staining show ECM protein deposition e.g. collagen.

(c) Masson's trichrome stained aortic section highlighting disruption of elastin fibers in Brn-3b KO mutants by fragmented blue staining (*),compared with WT aortas. Images were captured using Hammamatsu Nanozoomer imaging system and shown at x5 and x40 magnification.

(d) (i) Quantification of TA thickness in representative aortic sections (ii) Graph showing differences in TA thickness in aortic sections from WT or Brn-3b mice, with each point representing the mean values from individual samples. Data represents mean and standard error of 8 independent aortas, (+/-SD) with significance (***p <0.001) determined by students t-test.

(e) Representative images showing immunostaining of Col1a1 in WT and Brn-3b KO aorta sections representative images of WT or Brn-3b KO aortic sections stained with col1a1 Ab.

(f) van Gieson staining of elastin fibres (dark brown) in aortic section from WT or Brn-3b KO mice showing disruption of elastin fibres in Brn-3b KO aortas (arrowheads) when compared with WT aortas. Magnification is shown at 5X (top panels) and 40 X magnification (bottom).

Fig 3: Transmission electron microscopy images showing differences between aortas taken from WT and Brn-3b KO mice.

(a) Increased collagen fibres in the Tunica adventitial (TA) layer with Brn-3b KO aortas showing significantly thicker TA with more compact arrangement of collagen fibres when compared with WT controls.

(b) Representative images of the tunica media (TA) showing elastin fibres and VSMCs found between the elastic fibres (E) are indicated. Disruption of elastin fibres in Brn-3b KO aortas are indicated by yellow arrows, when compared with WT aortas.

(c) Images showing aortic perivascular adipose tissue (PVAT) surrounding the aorta taken from either WT or Brn-3b KO mice. Black arrows indicate larger numbers of infiltrating lymphocytes in Brn-3b KO PVAT when compared with WT controls.

Figure 4: Analysing contractile responses in vascular rings from Brn-3b KO aortas

(a+b) Echocardiography data showing changes in ascending aortic velocity (a) and measurement of aortic root diameter in male Brn-3b KO mice, when compared with age-

matched WT controls (c) Graph showing IC100 measurement (from wire myography) that was used to measure elastic properties of vascular rings from WT and Brn-3b KO mice at baseline. (d) Summary of data showing responses of thoracic aortic vascular rings from Brn-3b KO aortas and WT controls, following treatment with cumulative concentration of (i) KCl, (ii) PE and (iii) PGH2 prostaglandin analogue, u46619. Graphs show changes in force of contraction (DmN) elicited following different treatments, as shown. Data represents mean and standard error of measurements from vascular rings taken from 6 independent Brn-3b KO and WT aortas. Statistical significance was determined using two-way ANOVA analysis.

Figure 5: Analysis of RNA seq data using iDEP9.1 software:

(a) Principal Component Analysis (PCA) of all data obtained from RNA sequencing of WT and Brn-3b KO aortas. Samples from all 3 KO aortas (orange dots) were clustered together (boxed area) but only 2 WT samples (oval) showed similar patters while the WT sample 2M (circled), was identified as an outlier with significant differences in both PC1 and PC3 components and was excluded from analyses. (b) Heat map showing the 4 clusters arising from K-means clustering of the top 2500 from 2 WT and 3 KO samples (excluding outlier sample, 2M WT). KEGG pathways associated with enriched genes within each cluster are shown i.e. Red = upregulated genes; green = down regulated genes.

Fig 6: Summary of data obtained from DEG2 analysis differentially expressed genes in Brn-3b KO aortas when compared with WT controls

(a) Heat map showing differential expression of genes (DEG) in Brn-3b KO aortas, compared with WT controls- down-regulated = top panel; up-regulated = bottom panel.

(b) VENN diagram showing the numbers of up and down-regulated genes, using FDR cut-off = 0.1; fold change =1.5

(c) Schematic diagram showing how genes that are up-regulated or down-regulated in Brn-3b KO aortas are linked in the calcium signalling pathway. Image was rendered as a modified KEGG graph in Pathview with red boxes indicating genes that were increased in Brn-3b KO aortas while green boxes indicate decreased genes and gray indicate unchanged expression.

Fig 7a: Validation of selected differentially regulated genes from RNA sequencing data by qRT-PCR.

(a) Selected genes showing differential expression in Brn-3b KO aortas (n = 3) compared with WT aortas (n= 2) in RNA sequencing analysis.

(b) qRT-PCR validation of selected genes that were upregulated in Brn-3b KO mutants when compared with WT controls or

(c) reduced in Brn-3b KO mutants when compared with WT controls.

Variation between RNA samples was adjusted using 36B4 or GAPDH and values are expressed as fold changes relative to reference samples included in each experiment. Data represent mean (± sd) from n = 8-10 independent samples with statistical analysis undertaken using students t-test (*$p<0.05$).

Figure 8: Proposed mechanism by which gene expression changes caused by loss of Brn-3b may affect VSMC fate and function and thereby vascular contractility: (a) Schematic diagram of Ca2+ regulation of contraction and S/ER stress responses in normal contractile VSMC. (b) Effects caused by loss of Brn-3b which caused changes in selected genes that regulate Ca2+ signalling or stress responses in Brn-3b KO VSMC. Genes up-regulated in Brn-3b KO cells are shown in red and down-regulated genes in blue. **‘**X’ indicate inhibition of function or loss of expression. *Images created in by Biorender*

Table 1: Summary of Gene Set Enrichment Analysis (GSEA) used to identify pathways affected by loss of Brn-3b in the aorta:

GSEA data showing functional KEGG pathways associated with genes that were either (a) upregulated or (b) down regulated in Brn-3b KO aortas, when compared with WT controls. Significance was determined using the normalisation enrichment scores (NES), number of genes and adjusted p-value. NES [(+) = increased expression; (-) = down-regulated genes in Brn-3b KO tissue. (c) Summary of Jensen disease pathway analysis to identify effects caused by genes that were significantly and when compared with WT controls differentially expressed genes in Brn-3b KO mutants

Table 2: Selected genes that were differentially regulated in Brn-3b KO aortas

(a) Selected upregulated genes that in male Brn-3b KO aortas are grouped according to key known function; log-2-fold change [with (+) indicating upregulation and (-) downregulation]; ENSEMBL ID and brief description of each gene.

(b) List of selected genes that were down-regulated in male Brn-3b KO aortas.

Supplementary data

S-Fig 1: Western blot used to produce Fig 1a is shown in full. This also includes positive control samples prepared from mouse testis, known to express Brn-3b.

S-Table 1: (a) List of genes upregulated in Brn-3b KO aortas that are linked to muscle contractility and/or Ca2+ signalling or (b) metabolic responses; immune response pathways or circadian processes. Arranged by number of genes, with significance indicated by normalisation enrichment scores (NES) and adjusted p-value to indicate significance.

S-Table 2: (a) List of GO biological processes or (b) cellular components, associated with enriched genes within each cluster using data from 2 WT and 3 Brn-3b KO. Adjusted p-value and number of genes associated with different pathways are shown for each cluster

Figures

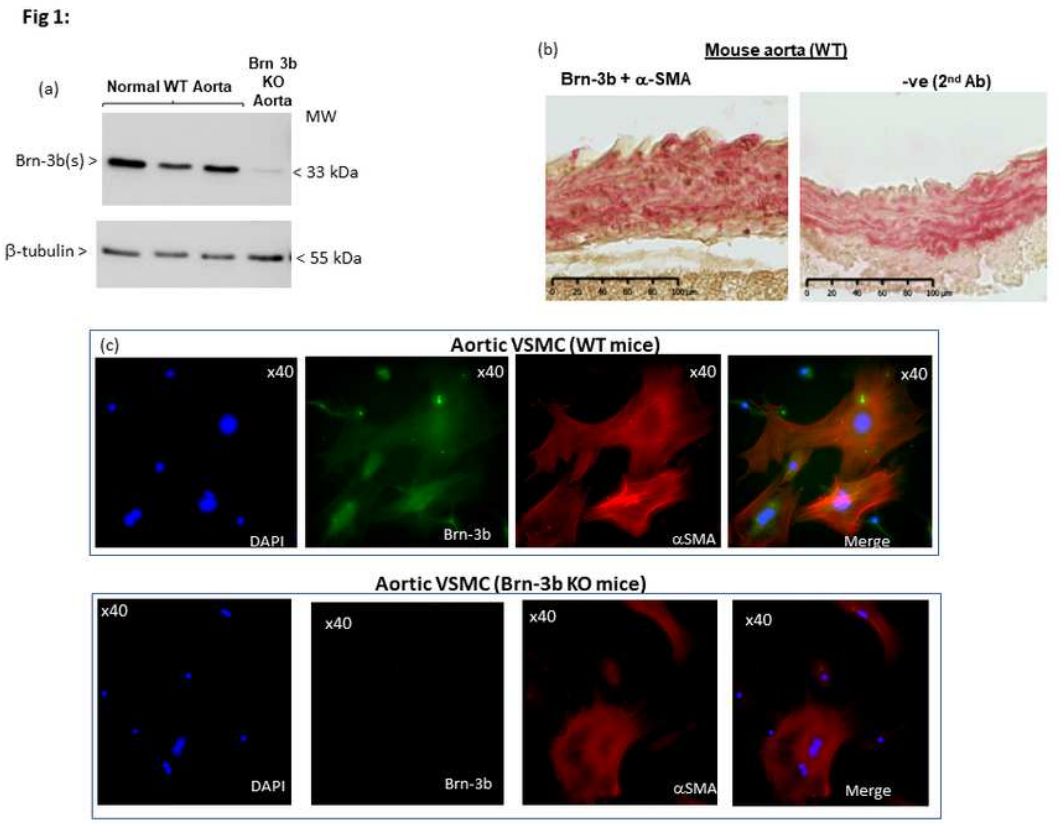

Figure 1

Brn-3b expression in aortic protein extracts and VSMC cultures.

(a) WB showing Brn-3b protein in WT mouse aortic extracts, compared with Brn-3b KO aortic extracts (negative control). b-tubulin blots indicate variation in protein loading. (b) Representative images of immunostained WT aortic sections showing co-localisation of Brn-3b (brown) with VSMC marker, aSMA (magenta). Negative control = 2nd Ab and a-SMA. (c) Representative immunofluorescent images of aortic VSMCs from WT moice (top panel) or Brn-3b KO mice, co-stained with Brn-3b (green) and a-SMA (red). DAPI mount indicates cell nuclei (blue).

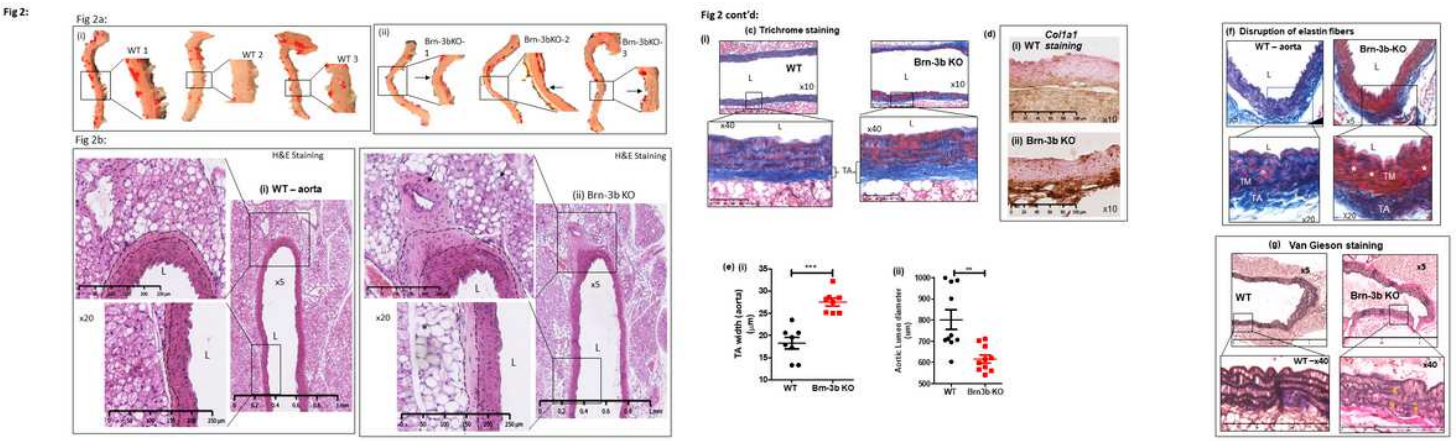

Figure 2

Histological changes in Brn-3b KO aorta when compared with WT controls

(a) Representative images of intact aortas taken from WT or Brn-3b KO mice, after staining for oil red. Images shown at X5 magnification with boxed areas expanded to highlight narrowing/constriction in Brn-3b KO aortas and corresponding WT aortas.

(b) H&E staining of longitudinal aortic sections from WT (i) or Brn-3b KO mice (ii). X20 magnification of selected areas shows increased adventitial thickness highlighted by dotted lines (arrows indicate specific areas of thickening in KO aortas; * highlights increased WAT deposition). L = lumen.

(c) Representative images showing Masson's trichrome staining of longitudinal aortic sections from either (i) WT or (ii) Brn-3b KO mice which highlights the increases in TA thickness (rounded brackets) and areas with elastin disruption in Brn-3b KO aortas (*). Red staining represent cytoplasm staining; dark purple/black indicates cell nuclei; blue staining show ECM protein deposition e.g. collagen.

(d) Masson's trichrome stained aortic section highlighting disruption of elastin fibers in Brn-3b KO mutants by fragmented blue staining (*),compared with WT aortas. Images were captured using Hammamatsu Nanozoomer imaging system and shown at x5 and x40 magnification.

(e) (i) Quantification of TA thickness in representative aortic sections (ii) Graph showing differences in TA thickness in aortic sections from WT or Brn-3b mice, with each point representing the mean values from individual samples. Data represents mean and standard error of 8 independent aortas, (+/-SD) with significance (***p <0.001) determined by students t-test.

(f) Representative images showing immunostaining of Col1a1 in WT and Brn-3b KO aorta sections representative images of WT or Brn-3b KO aortic sections stained with col1a1 Ab.

(g) van Gieson staining of elastin fibres (dark brown) in aortic section from WT or Brn-3b KO mice showing disruption of elastin fibres in Brn-3b KO aortas (arrowheads) when compared with WT aortas. Magnification is shown at 5X (top panels) and 40 X magnification (bottom panels).

Fig 3:

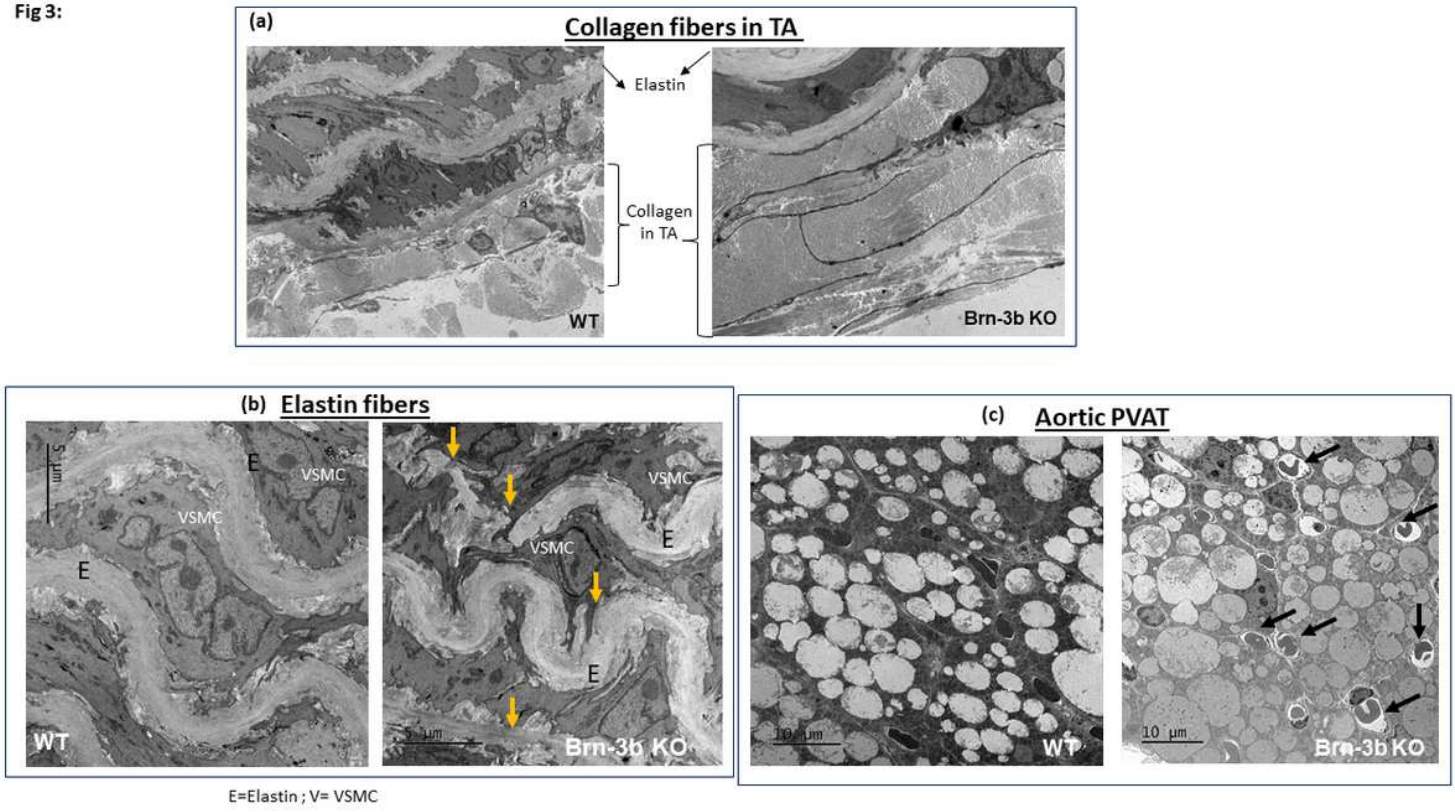

Figure 3

Transmission electron microscopy images showing differences between aortas taken from WT and Brn-3b KO mice.

(a) Increased collagen fibres in the Tunica adventitial (TA) layer with Brn-3b KO aortas showing significantly thicker TA with more compact arrangement of collagen fibres when compared with WT controls.

(b) Representative images of the tunica media (TA) showing elastin fibres and VSMCs found between the elastic fibres (E) are indicated. Disruption of elastin fibres in Brn-3b KO aortas are indicated by yellow arrows, when compared with WT aortas.

(c) Images showing aortic perivascular adipose tissue (PVAT) surrounding the aorta taken from either WT or Brn-3b KO mice. Black arrows indicate larger numbers of infiltrating lymphocytes in Brn-3b KO PVAT when compared with WT controls.

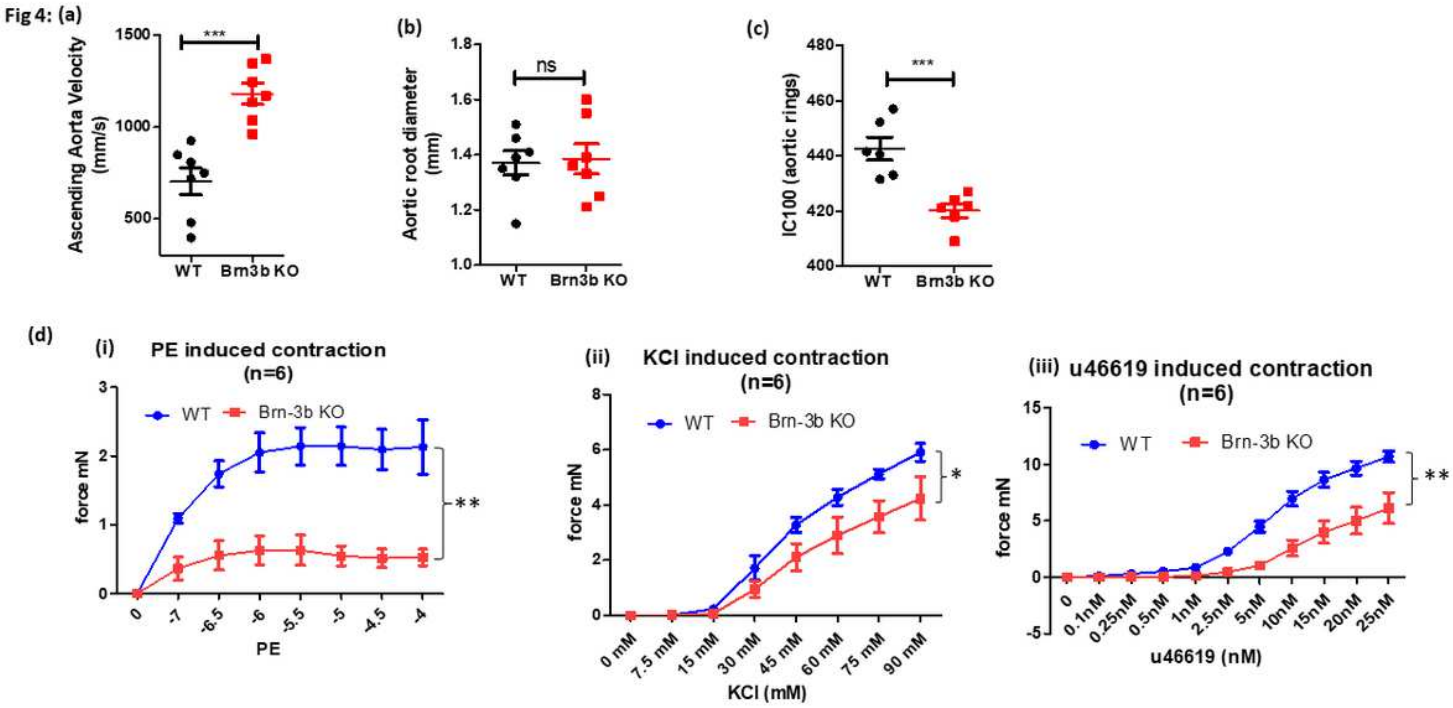

Figure 4

Analysing contractile responses in vascular rings from Brn-3b KO aortas

(a+b) Echocardiography data showing changes in ascending aortic velocity (a) and measurement of aortic root diameter in male Brn-3b KO mice, when compared with age-matched WT controls (c) Graph showing IC100 measurement (from wire myography) that was used to measure elastic properties of vascular rings from WT and Brn-3b KO mice at baseline. (d) Summary of data showing responses of thoracic aortic vascular rings from Brn-3b KO aortas and WT controls, following treatment with cumulative concentration of (i) KCl, (ii) PE and (iii) PGH2 prostaglandin analogue, u46619. Graphs show changes in force of contraction (DmN) elicited following different treatments, as shown. Data represents mean and standard error of measurements from vascular rings taken from 6 independent Brn-3b KO and WT aortas. Statistical significance was determined using two-way ANOVA analysis.

Fig 5:

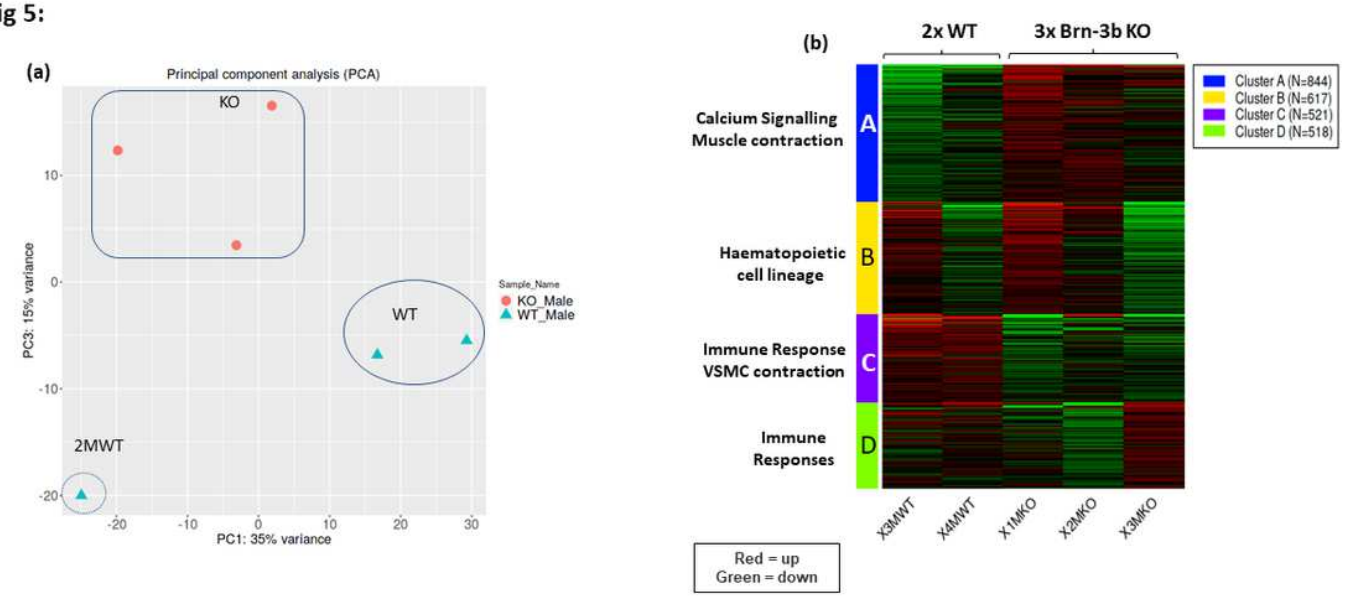

Figure 5

Analysis of RNA seq data using iDEP9.1 software:

(a) Principal Component Analysis (PCA) of all data obtained from RNA sequencing of WT and Brn-3b KO aortas. Samples from all 3 KO aortas (orange dots) were clustered together (boxed area) but only 2 WT samples (oval) showed similar patters while the WT sample 2M (circled), was identified as an outlier with significant differences in both PC1 and PC3 components and was excluded from analyses. (b) Heat map showing the 4 clusters arising from K-means clustering of the top 2500 from 2 WT and 3 KO samples (excluding outlier sample, 2M WT). KEGG pathways associated with enriched genes within each cluster are shown i.e. Red = upregulated genes; green = down regulated genes.

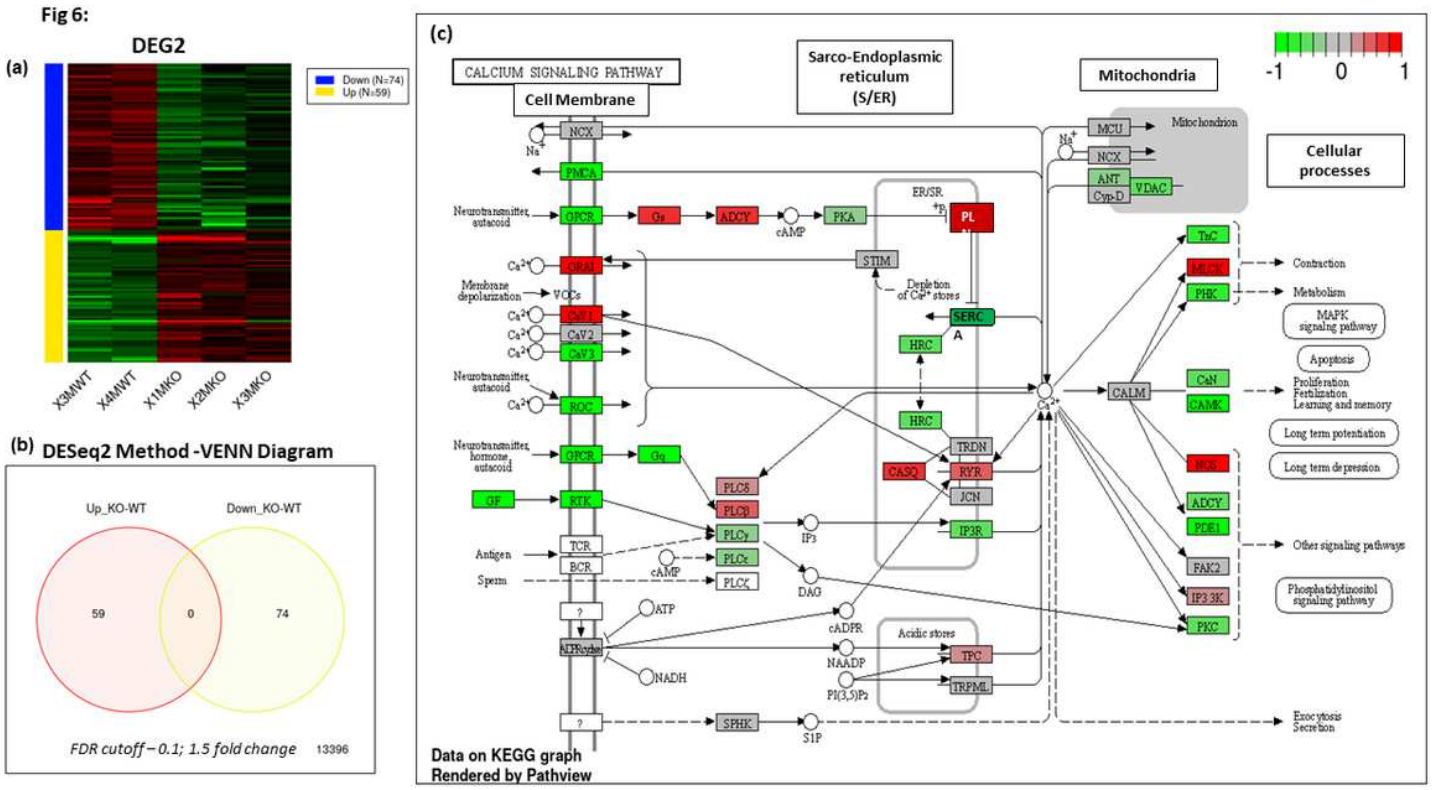

Figure 6

Summary of data obtained from DEG2 analysis differentially expressed genes in Brn-3b KO aortas when compared with WT controls

(a) Heat map showing differential expression of genes (DEG) in Brn-3b KO aortas, compared with WT controls- down-regulated = top panel; up-regulated = bottom panel.

(b) VENN diagram showing the numbers of up and down-regulated genes, using FDR cut-off = 0.1; fold change =1.5

(c) Schematic diagram showing how genes that are up-regulated or down-regulated in Brn-3b KO aortas are linked in the calcium signalling pathway. Image was rendered as a modified KEGG graph in Pathview with red boxes indicating genes that were increased in Brn-3b KO aortas while green boxes indicate decreased genes and gray indicate unchanged expression.

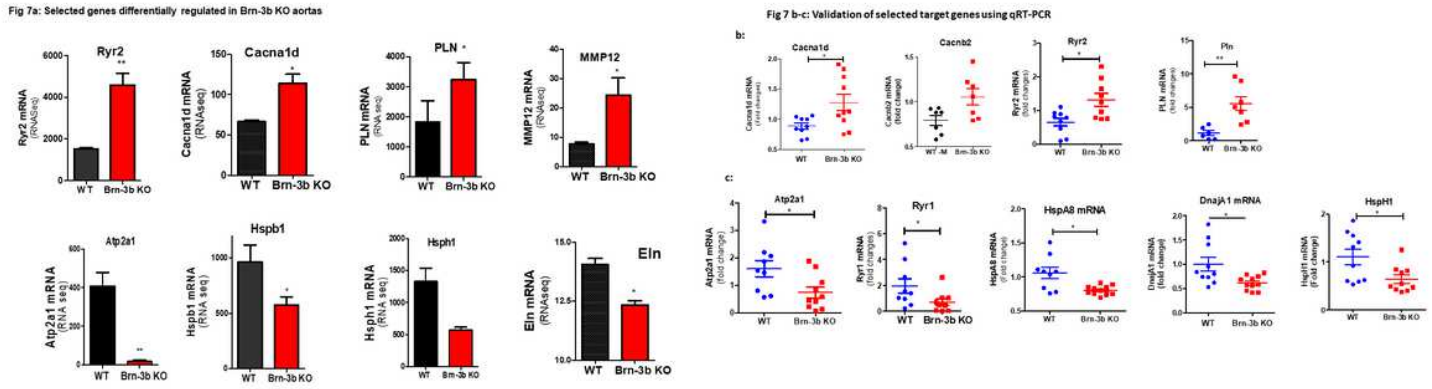

Figure 7

Validation of selected differentially regulated genes from RNA sequencing data by qRT-PCR.

(a) Selected genes showing differential expression in Brn-3b KO aortas (n = 3) compared with WT aortas (n= 2) in RNA sequencing analysis.

(b) qRT-PCR validation of selected genes that were upregulated in Brn-3b KO mutants when compared with WT controls or

(c) reduced in Brn-3b KO mutants when compared with WT controls.

Variation between RNA samples was adjusted using 36B4 or GAPDH and values are expressed as fold changes relative to reference samples included in each experiment. Data represent mean (± sd) from n = 8-10 independent samples with statistical analysis undertaken using students t-test (*p<0.05).

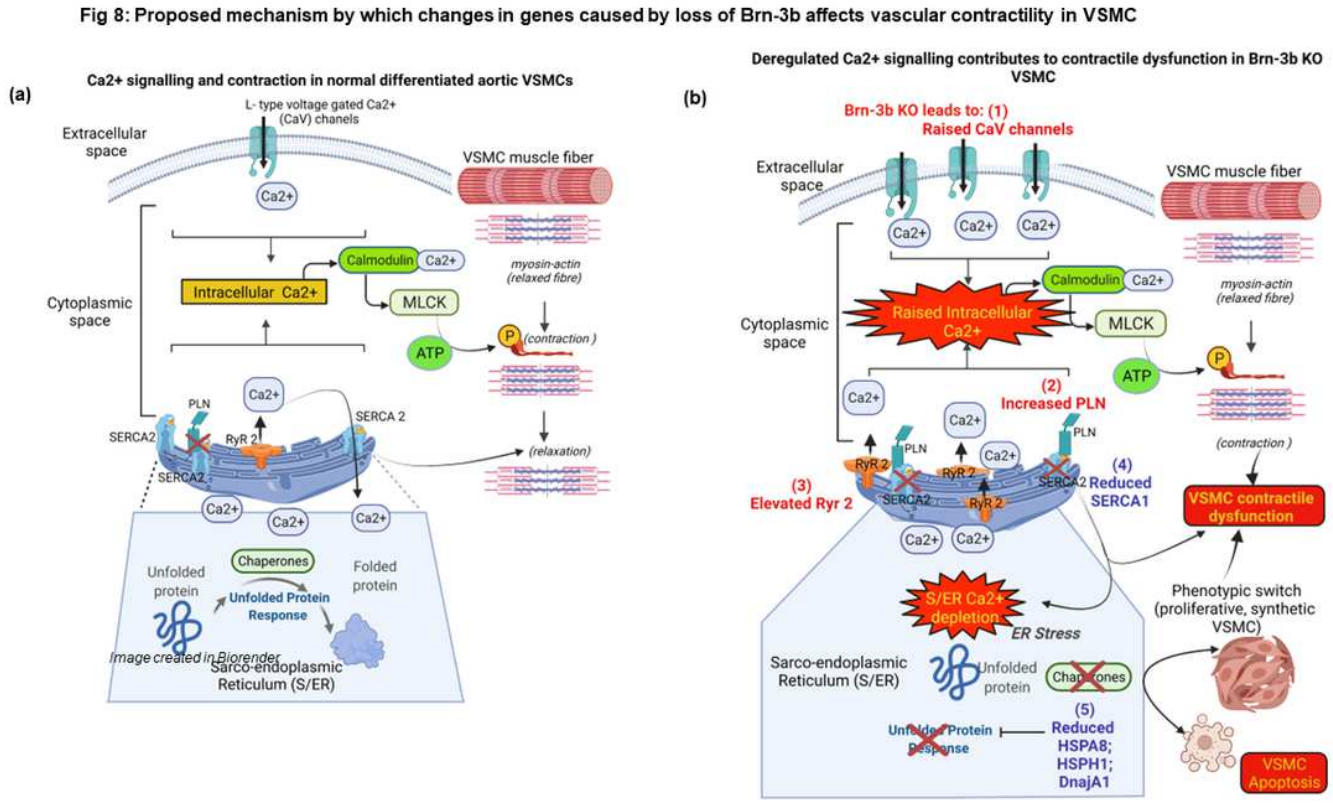

Figure 8

Proposed mechanism by which gene expression changes caused by loss of Brn-3b may affect VSMC fate and function and thereby vascular contractility: (a) Schematic diagram of Ca2+ regulation of contraction and S/ER stress responses in normal contractile VSMC. (b) Effects caused by loss of Brn-3b which caused changes in selected genes that regulate Ca2+ signalling or stress responses in Brn-3b KO VSMC. Genes up-regulated in Brn-3b KO cells are shown in red and down-regulated genes in blue. 'X' indicate inhibition of function or loss of expression. *Images created in by Biorender*

Supplementary Files

This is a list of supplementary files associated with this preprint. Click to download.

- Table1.png
- Table2.png
- Brn3bvascularpaperFigures2023CDDissupplementaryfigsfinal.pdf
- SupplementarydataInfo.docx